Politecnico di Torino

Politecnico di Torino

Master's Degree in Biomedical Engineering

Evaluation of Cardiac Adaptation in Patients Undergoing Passive Leg Raising (PLR) Maneuvers: Inferior Vena Cava Study

Supervisors:
Prof. Luca Mesin
Ing. Piero Policastro

Candidate:
Camilla De Robertis

Academic Year 2023/24

Abstract

Passive leg raising (PLR) maneuver is a non-invasive and effective technique to assess fluid responsiveness, particularly useful in monitoring cardiac preload. Unlike intravenous administration, which involves direct fluid introduction and potential associated risks, PLR allows immediate assessment by simulating the effect of a fluid load without actual infusion.
In this study, thirteen healthy subjects (5 men and 8 women, mean age 27 ± 9.5 years) underwent two consecutive PLR maneuvers. Each maneuver was assessed through a sequence of three events: pre-maneuver (baseline), during PLR and immediately after the maneuver.
Segmentation of the inferior vena cava (IVC) was performed using software developed by Viper s.r.l., which included the use of a GUI in MATLAB for data analysis. A graphical user interface (GUI) was then developed in Python, using the PyQt6 library, to further facilitate the use of the software.
Segmentation allowed the analysis of parameters indicative of hemodynamic behavior, such as inferior vena cava diameter, caval index (CI), cardiac caval index (CCI), and respiratory caval index (RCI).
During the first maneuver, the mean inferior vena cava diameter increased from a baseline value of 14.4 ± 4.7 mm to 16.6 ± 4.1 mm during PLR, subsequently decreasing to 14.9 ± 5.1 mm after the maneuver. Correspondingly, the caval index (CI) showed an inverse change, decreasing from 0.35 ± 0.13 to 0.26 ± 0.01 during PLR and returning to 0.34 ± 0.12 after the maneuver. For the second maneuver, the inferior vena cava diameter increased from 13.7 ± 5.0 mm (before the maneuver) to 16.8 ± 5.3 mm during PLR, then decreased to 13.3 ± 4.4 mm after the maneuver, with a corresponding decrease in CI from 0.33 ± 0.13 to 0.26 ± 0.01, and then returned to 0.34 ± 0.13. The mean interval between the two maneuvers was 23.82 ± 3.47 minutes.
This study evaluated the correlations between pulsatility indices and mean diameters in various observation periods using two-way ANOVA and paired-sample t-test. Two-way ANOVA revealed significant differences between time states, indicating that these states significantly influence both pulsatility indices and diameters. However, no significant intra-subject differences were observed. Two-sample t-tests demonstrated significant differences between parameters calculated during both PLR maneuvers and their respective baselines, as well as immediately following intervals, but no significant differences were found between parameters calculated during the two maneuvers.
In conclusion, the results indicate that the passive leg raising (PLR) maneuver does not lead to physiological adaptation, affirming that the PLR is a consistent, reliable, and repeatable measure over time. This analysis suggests that the PLR can effectively assess fluid responsiveness in clinical settings without the influence of previous tests.

Acknowledgements

In this section I would like to express my gratitude to the people and organizations that contributed to the completion of the thesis. I am deeply grateful to Professor Luca Mesin for giving me the opportunity to work on this project and for having placed his trust in a positive outcome of the activity.
I am equally grateful to Piero Policastro for having guaranteed me constant support, for having always listened to my point of view and for always having put me in a position to carry out my work to the best of my abilities.

Contents

List of Figures

List of Tables

Chapter 1

Introduction

Segmentation of the inferior vena cava (IVC) using ultrasound is essential for evaluating the clinical status of patients, particularly regarding fluid volume and right atrial pressure (RAP). In recent years, the use of IVC in clinical settings has gained considerable attention, as it allows for non-invasive and continuous monitoring of the hemodynamic response. Segmentation of the IVC allows a detailed analysis of its dimensions and allows the calculation of pulsatility parameters, including the Caval Index (CI), the Cardiac Caval Index (CCI) and the Respiratory Caval Index (RCI). However, despite growing interest, gaps still exist in understanding changes in these parameters, especially when analyzed in specific clinical contexts, such as during maneuvers such as Passive Leg Raising (PLR). The PLR maneuver, in fact, is a non-invasive method that allows the patient's hemodynamic response to postural changes to be assessed and can provide valuable information on the adaptive capacity of the cardiovascular system. Therefore, the present study aims to examine the robustness of these indices and their ability to reflect the hemodynamic response to PLR-induced changes. Through the segmentation of the IVC in thirteen healthy subjects, during this thesis work we attempted to analyze the changes in the hemodynamic parameters induced by two PLR maneuvers performed a few minutes apart from each other, using the software developed by Viper s.r.l., which allows precise measurement of the size and pulsatility of the vein. The results obtained could have significant implications for the optimization of non-invasive hemodynamic monitoring, paving the way towards future clinical research.

Chapter 2

Background

2.1 Cardiovascular system

The cardiovascular system is a closed system of blood vessels in which blood circulates thanks to the heart's pumping action. The cardiovascular system is defined as double and complete: double, because with each circulatory act, blood passes through the heart twice; complete, because oxygenated and non-oxygenated blood never mix. There are two types of circulation:

- Systemic circulation or large circulation: It originates in the left ventricle of the heart and allows the transport, through the blood, of oxygen and other metabolites to all body tissues, as well as the removal of carbon dioxide and other wastes.
- Pulmonary circulation or small circulation: It originates in the right ventricle of the heart and allows the transport of deoxygenated blood to the lungs, where it is oxygenated before being carried to the left atrium of the heart.

The complex network of vessels that form the cardiovascular system is composed of various blood vessels, such as arteries, veins, and microcirculation, the latter consisting of capillaries, arterioles, and venules.

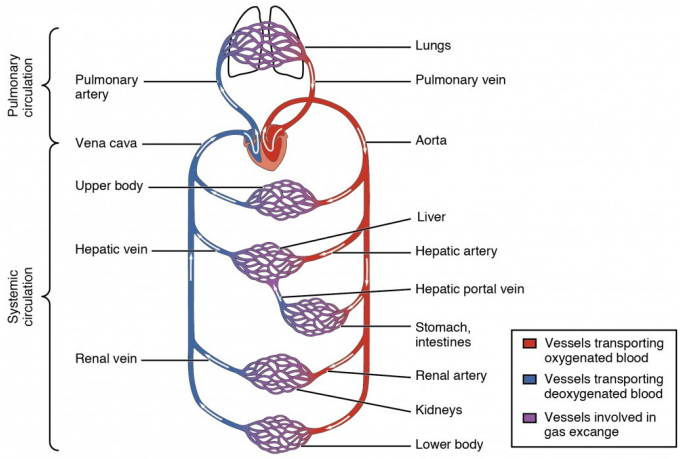

Figure 2.1: The circulation of blood through the heart [8].

2.2 Cardiac cycle

The heart is a pump whose function is to transport oxygen-rich blood to cells, tissues, and organs to nourish them, and to receive carbon dioxide-laden blood, which is then sent to the lungs where the exchange with oxygen takes place. Oxygenated blood, or arterial blood, travels through the body via the aorta, while deoxygenated blood, which contains metabolic waste products from the cells, returns to the heart through the vena cava. At rest, the heart can supply approximately 5 liters of oxygenated blood per minute. The heart ensures continuous blood circulation through coordinated movements, consisting of two phases that repeat on average 70-80 times per minute at rest:

- Systole: This is a phase of myocardial contraction. During the ventricular systole phase, the semilunar valves open due to the contraction of the ventricular chamber, which pushes blood into the aorta, while the atrioventricular valves close.
- Diastole: This is a phase of myocardial relaxation. During the ventricular diastole phase, the valves between the atria and ventricles are open, the musculature of the ventricular chamber is relaxed, and blood passively flows from the atria to the ventricles. The semilunar valves remain closed. During this phase, the pressure decreases.

The valves open thanks to a pressure gradient. The atrioventricular valves, in particular, are open when there is a higher pressure in the atrium than in the ventricle, and closed when the opposite occurs. They separate the atria from the ventricles and ensure the unidirectional flow of blood from the atrium to the ventricle. The right atrioventricular valve is the tricuspid valve, while the left is the bicuspid valve, also known as the mitral valve. The semilunar valves allow blood to pass from the ventricles to the large arteries and are divided into two types: one separates the heart from the aorta (aortic valve) and the other separates the heart from the pulmonary artery (pulmonary valve).

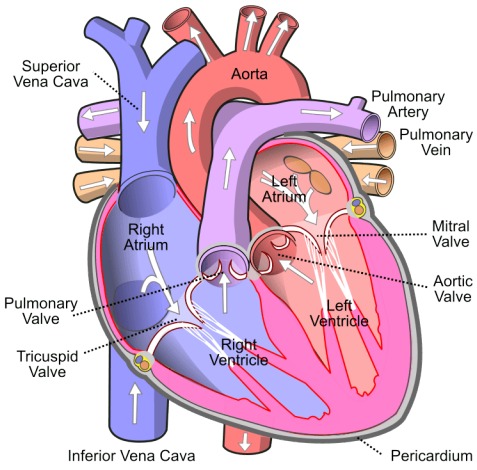

Figure 2.2: Cardiac structures [7].

2.3 Arterial system

In the cardiovascular system, arteries are the blood vessels responsible for transporting oxygen-rich blood from the heart to all tissues, with the exception of the pulmonary arteries, which carry carbon dioxide-laden blood and waste products, and the umbilical arteries, which are involved in forming the fetal placental circulation.
The arterial system is the part of the cardiovascular system characterized by high pressure. This pressure reaches its maximum value, known as systolic pressure, when the heart contracts and pumps blood into the arteries, and its minimum value, known as diastolic pressure, when the heart expands and refills with blood. The high pressure to which these vessels are subjected affects their anatomical structure, which is primarily characterized by elasticity and strength, and consists of three concentric layers:

- The intima is the innermost layer facing the lumen of the vessel and is composed of a thin layer of endothelial cells supported by a small layer of connective tissue. It plays a structural role and regulates the exchange of materials between the blood and tissues.
- The media consists of smooth muscle fibers and elastic fibers, which provide the vessel with elasticity and contractility.
- The adventitia or external layer is made up of loose connective tissue and bundles of smooth muscle fibers. Its primary function is to provide structural support [21].

Elastic laminae separate the layers from each other. This complex structure allows the vessels to withstand mechanical stress from systolic pressure (about 120 mmHg), as they are stretched and then return to their original dimensions due to their elasticity, thereby maintaining blood flow. The tunica media is the component that

determines the behavior and structure of the arteries, allowing them to be classified into three main categories:

- Large caliber arteries (elastic arteries): they have a diameter greater than 7 mm and are characterized by a prevalence of elastic tissue in the tunica media.
- Medium caliber arteries (muscular arteries): they have a diameter between 2.5 mm and 7 mm, and their structure is dominated by smooth muscle fibers which give greater control over blood flow.
- Small caliber arteries (arterioles): they have a diameter of less than 2.5 mm and play a fundamental role in the regulation of blood pressure and capillary flow thanks to the presence of a relatively large number of muscle cells in the tunica media.

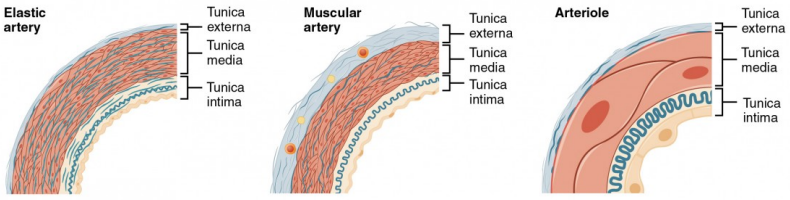

Figure 2.3: Structure and classification of arteries [8].

In the course of the arteries from the heart to the periphery, the caliber and elasticity of the latter progressively decreases, as does the pressure and the blood velocity. In the course towards the periphery, however, the muscular component increases. It is therefore easy to imagine that the change in the type of artery is very gradual; Thus, "transition zones" are characterized in which mixed arteries can be identified they present characteristics common to different vessel typologies. The flow of blood in the vessels is only possible when there is a pressure difference. Blood pressure, therefore, is the most important variable for the purposes of regulation of blood flow in the cardiovascular system

2.4 Venous system

Veins are blood vessels that transport blood from the body's peripheral areas back to the heart. Generally, veins carry oxygen-poor blood rich in carbon dioxide and waste products, except for the pulmonary veins, which transport oxygen-rich blood and nutrients from the lungs to the heart.
Veins, based on their diameter, are classified into: venous capillaries, venules, small-caliber veins, medium-caliber veins, and large-caliber veins. Their walls are made up of three concentric layers: the external tunic, the middle tunic, and the internal tunic. These walls are thinner than those of arteries, being characterized by a lower internal pressure, and have a predominance of the muscular component over the

elastic one.
The muscular component allows the veins to dilate as the amount of blood inside them increases. Some veins are equipped with one-way valves that promote blood flow toward the heart, preventing reflux. In the venous system of the lower limbs, in particular, muscular contractions play a crucial role in facilitating blood flow.
Venous return from the lower limbs to the heart is further influenced by respiratory variations, which alter the pressure gradients between the abdomen and the thoracic cavity [38]. This pressure differential is at its peak during deep inspiration, but it is present, albeit to a lesser extent, throughout the entire respiratory cycle [38].
Central Venous Pressure (CVP) represents a fundamental hemodynamic indicator that reflects the pressure in the thoracic vena cava, providing crucial information on venous return and cardiac preload. It represents a direct value of the amount of blood returning to the heart and the ability of the heart to pump blood effectively. In clinical settings, CVP is used to assess a patient's volumetric status, helping to identify conditions such as hypovolemia, fluid overload, and heart failure [31].

2.4.1 Vena cava

The vena cava divides into the superior vena cava (SVC) and the inferior vena cava (IVC); these are among the main structures of the venous system. The superior vena cava is a large venous trunk that carries oxygen-poor blood from the upper parts of the body (including the head, neck, upper limbs, and some thoracic organs) to the heart. It has a wide diameter of up to 2 cm and a length of approximately 7 cm [6].
The inferior vena cava is located within the abdominal cavity and traverses the thoracic diaphragm through the caval opening to connect with the right atrium of the heart. It is the largest venous trunk in the human body, responsible for returning oxygen-poor blood from the lower parts of the body (including the lower limbs and all organs located below the diaphragm) to the heart. It has an average length of about 22 cm, with 18 cm of this extending through the abdomen, and has a diameter of roughly 30 mm [14]. Its size and collapsibility are crucial indicators that reflect the right atrial pressure (RAP) and fluid distribution within the venous system.
It is therefore clear that the analysis of the vena cava is fundamental for understanding the state of health of a patient. Furthermore, it is further significant to relate characteristic indicators of the IVC with other hemodynamic parameters, such as cardiac output (CO) and central venous pressure (CVP). CO represents the volume of blood pumped by the heart in one minute and is influenced by the amount of blood returning to the heart through the vena cava. Similarly, CVP provides crucial information about the pressure in the central venous system, reflecting the capacity of the right ventricle to accommodate blood. Monitoring these parameters combined with vena cava analysis is particularly relevant in critical clinical situations, where changes in venous pressure and cardiac output may indicate significant changes in the patient's hemodynamic status [33].

2.5 Respiratory system

The respiratory system consists of the organs and structures responsible for breathing and therefore for gas exchange between the external environment and the human body. Its main function is to provide oxygen to cells and remove metabolic waste, such as carbon dioxide. It is made up of several key components:

- Upper respiratory passages (nasal cavity, mouth, pharynx).
- Respiratory tract (larynx, trachea).
- Lungs.

Air first enters the body through either the nose or mouth, traveling through the pharynx before passing into the larynx. From there, it moves into the trachea and flows into the primary bronchi. Once inside the lungs, these bronchi branch out into progressively smaller airways, eventually leading to the bronchioles. At the very end of the bronchioles lie the pulmonary alveoli, elastic structures that can easily change shape and size. The alveoli, in fact, are coated with a substance called surfactant that allows them to expand and contract easily, helping the lungs and breathing and reducing the work required to breathe [3]. Each alveolus is made up of a network of capillaries containing blood rich in carbon dioxide and poor in oxygen. It is precisely at the level of this network of capillaries that the actual exchange of oxygen and carbon dioxide between the air and the blood flow in the capillaries occurs.
The ability to breathe, or the ability to take air into the lungs during inhalation and exhale during exhalation, depends on three types of pressure: atmospheric, intra-alveolar, and intrapleural. Intra-alveolar or intrapulmonary pressure is the pressure inside the alveoli that changes during the different phases of breathing. Because the alveoli are connected to the atmosphere by airway tubes, intrapulmonary pressure is always equal to atmospheric pressure. Intrapleural pressure is the air pressure between the visceral and parietal pleura and changes during the different phases of breathing. It is always lower or negative than intrapulmonary pressure, and therefore also lower than atmospheric pressure, with a value of about -4 mmHg throughout the respiratory cycle [2].
An additional pressure is determined by the difference between the intrapleural and intrapulmonary pressure, called the transpulmonary pressure, which determines the size of the lungs: the higher the transpulmonary pressure, the larger the size of the lung.

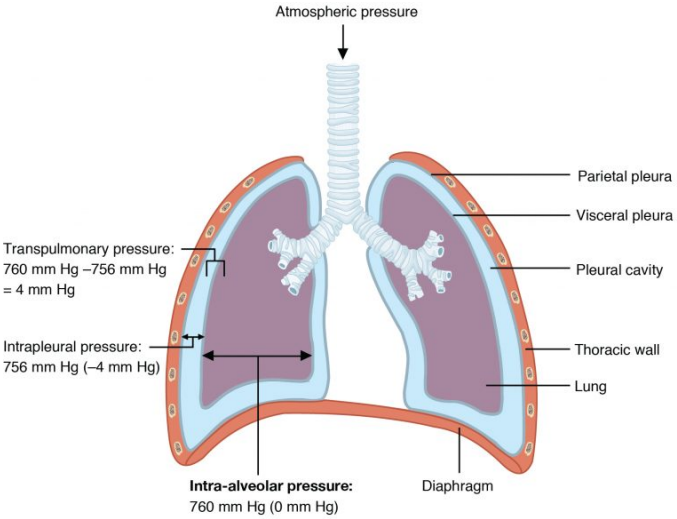

Figure 2.4: Relationships between intrapulmonary and intrapleural pressure [1]

In addition to the differences in pressure, breathing depends on the relaxation and contraction of the muscle fibers of the diaphragm and chest. This is because the lungs are passive during breathing, as their expansion and contraction is guaranteed by the adhesive nature of the pleural fluid that allows the lungs to be pulled outward when the chest wall moves during inspiration and to contract during expiration [2].

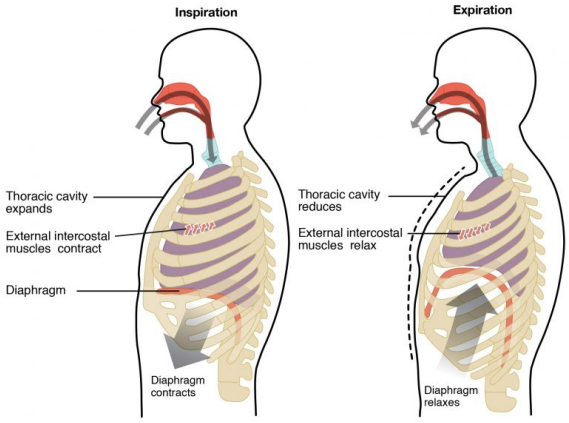

Figure 2.5: Phases of inhalation and exhalation [1].

Chapter 3

Ultrasonography

Ultrasound is an imaging technique that uses ultrasound waves, which are high-frequency mechanical waves, to interact with tissues and generate two-dimensional images. The frequencies of these acoustic waves are higher than what the human ear can perceive; while the human ear can hear frequencies up to 20 kHz, the frequency range produced by an ultrasound machine is between 2 MHz and 20 MHz. There are two main reasons why this imaging technique holds a prominent position in the field of medical imaging:

- It uses a form of energy that is not particularly dangerous, allowing prolonged use of these devices for measurements.
- It is characterized by very high temporal resolution, meaning it can observe dynamic phenomena.

3.1 Ultrasound physics

Acoustic waves propagate through a medium by utilizing the mechanism of compression and rarefaction. However, the speed at which acoustic waves travel depends on the medium they are passing through. In general, the propagation speed of a wave in a medium is described by the following relationship:

$$v = \lambda \times \mathrm{f} \tag{3.1.1}$$

where λ is the wavelength and f is the frequency of the wave. In ultrasound devices, the speed of sound propagation is set to a value of 1540 m/s. The fundamental quantity that governs the propagation of ultrasound in tissues, denoted as Z, is the acoustic impedance, which refers to the tendency of sound waves to propagate in one tissue rather than another. This quantity is given by the product of the density of the propagation medium and the speed of propagation within it.

$$Z = \rho \times v \tag{3.1.2}$$

This parameter varies among the different tissues of the human body.

Material	**Density** (kgm^{-3})	**Propagation Velocity** (ms^{-1})	**Acoustic Impedance** ($kgm^{-2}s^{-1} \cdot 10^6$)
Air	1.2	330	0.0004
Water	1000	1480	1.48
Soft tissue	1060	1540	1.63
Muscle	1080	1580	1.70
Fat	952	1459	1.38
Brain	994	1560	1.55
Kidney	1038	1560	1.62
Lung	400	650	0.26
Bone	1912	4080	7.80

Table 3.1: Acoustic properties of air, water and biological tissues.

In the context of ultrasound, the term 'soft tissue' does not refer to a single specific tissue, but rather to an approximation based on the averaged acoustic properties of various tissues, such as muscle, fat, and internal organs. This allows for a unified definition of tissues with similar acoustic characteristics. For this group of tissues, an average density of 1060 kg/m^3 and a sound propagation speed of 1540 m/s are assigned to simplify diagnostic imaging. The physics of ultrasound is based on the principle of reflection. When a sound wave propagates through a non-homogeneous tissue, meaning with different acoustic impedances, it is partially reflected at the junction between the two tissues.

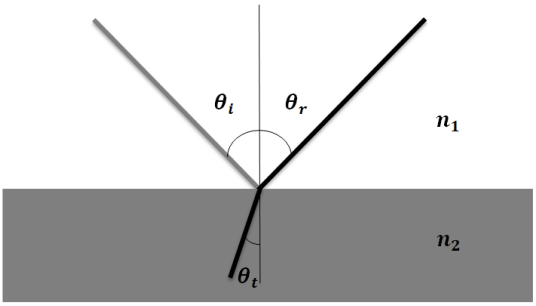

Figure 3.1: Propagation of sound waves

The amount of the wave that will be reflected depends on a coefficient, called the reflection coefficient:

$$R = \left(\frac{Z_1 \cos(\theta_t) - Z_2 \cos(\theta_r)}{Z_1 \cos(\theta_t) + Z_2 \cos(\theta_r)} \right)^2 \tag{3.1.3}$$

where Z_1 is the acoustic impedance of the first tissue, Z_2 is the acoustic impedance of the second tissue, θ_r is the reflection angle of the acoustic wave and θ_t is the transmission angle of the acoustic wave. It is possible to define another coefficient,

known as transmission coefficient, which complements the reflection coefficient:

$$T = 1 - R \tag{3.1.4}$$

In ultrasonography, a simplifying assumption is made, namely, that the radiation arrives at the discontinuity always orthogonal to it. This means that the cosine values are equal to one, and the definition of the reflection coefficient simplifies, depending only on the values of the acoustic impedances of the two media.

$$R = \left(\frac{Z_1 - Z_2}{Z_1 + Z_2}\right)^2 \tag{3.1.5}$$

The reflection coefficient takes on a unitary value when the entire wave is reflected, generating a white image, and it is zero when the two acoustic impedances are equal, which occurs when the wave propagates through a homogeneous tissue. However, it is always important to consider the wavelength of the acoustic waves used in ultrasonography, because human blood, for example, is not a homogeneous tissue, but a mixture of liquid and corpuscular parts, with red blood cells as the main component. Since red blood cells have dimensions between 5 and 10 micrometers, it is not possible for the ultrasound to interact with them, as the wavelength of the ultrasound used in imaging is around 70 micrometers. This is why blood, although inhomogeneous, does not produce reflections in ultrasound images and appears black. The acoustic wave is, however, also attenuated by the tissue in which it travels. The energy of the wave is, in fact, partly absorbed or scattered if the size of the particles and that of the wavelength are comparable) and decreases in amplitude according to the equation:

$$A(z) = A_0 e^{-\alpha z} \tag{3.1.6}$$

where A is the attenuated amplitude of the wave, A_0 is the initial amplitude of the wave, α is the attenuation coefficient and z is the distance traveled by the wave in the medium. Some media, such as lungs, air and bones, strongly attenuate US, acting as barriers to their propagation. It is important to note that the attenuation coefficient is a function of frequency. Specifically, as the frequency increases, the attenuation coefficient also increases. In ultrasonography, it would be more convenient to work with higher frequencies to achieve shorter wavelengths, thus providing better spatial resolution. However, increasing the frequency also increases attenuation, which is why a compromise is typically made, with a maximum frequency of 20 MHz.

3.2 Ultrasound generation principle

Ultrasounds are generated by elements capable of managing energy in a directional manner. This property is characteristic of certain crystals and is known as the phenomenon of piezoelectricity, which is fundamental to the generation of ultrasounds. Piezoelectricity can be direct or inverse.

- Direct piezoelectricity: If a crystal with piezoelectric properties undergoes a change in dimension in a specific direction, a variation in potential energy between its faces will occur. This variation is linear, the greater the geometric change, the greater the potential difference.

- Inverse piezoelectricity: If a crystal with piezoelectric properties is subjected to a change in potential energy between its faces, it will react by altering its geometric properties. To generate and detect ultrasounds, the inverse piezoelectric effect is utilized.

Supposing we want to use a piezoelectric crystal to generate an ultrasound at a frequency of 2 MHz, a potential difference in the form of a sine wave with a frequency of 2 MHz will be applied across the faces of the crystal. This sine wave will be characterized by a certain amplitude and frequency: the frequency of the sine wave determines the frequency of the acoustic field, while the amplitude of the sine wave reflects a higher or lower intensity of the acoustic field. In this way, ultrasounds are generated. To measure the returning echo to the probe, however, the direct piezoelectric effect is utilized. The piezoelectric crystal, in contact with the tissue, will receive the wave reflected from the discontinuity of the tissue at depth, and this wave will also be a sine wave at the same frequency but with a smaller amplitude. Ideally, it can be said that if the returning echo was generated by a discontinuity with a very high reflection coefficient, it will have a higher intensity, whereas if it was generated by a discontinuity with a very low reflection coefficient, it will have a lower intensity. The most commonly used piezoelectric crystal in the field of ultrasonography is lead zirconate titanate (PZT); it is, in fact, a linear ceramic that is easily machinable, has good mechanical durability, and is also moderately priced.

3.3 Image generation principle

The ultrasound image is a two-dimensional map of the distribution of tissue reflection coefficient values. The ultrasound probe is made up of a series of piezoelectric elements with a thickness of approximately 0.4 mm, each of which emits a pulse. Basically, of all the piezoelectric elements present in a probe, a few are used at a time to obtain a scan line. Typically the number of piezoelectric elements present in a probe ranges from 128 to 256. When the pulse encounters a discontinuity in the tissue, part of it is reflected, generating a return echo. By measuring the time of flight, that is the time between the emission of the pulse and the reception of the returning echo, it is possible to calculate the distance from the probe at which the echo was generated:

$$d = \frac{c \cdot \Delta t}{2} \tag{3.3.1}$$

Once you have calculated at what depth the discontinuity is present, it will be possible to convert the amplitude of the returning echo into color, at that depth, to form the ultrasound image. The amplitude of the returning echo will depend on the reflection coefficient but also on the attenuation due to propagation in the tissue. The only depth information necessary to create the image is intended to depend only on the reflection coefficient. There is a block in the device, called time gain compensation (TGC) which decouples the effect of the attenuation from the effect of the reflection coefficient. Currently, there are several types of probes available on the market, which can be divided into four main categories:

- Linear probes: the piezoelectric elements are arranged in a row.

- Convex probes: the piezoelectric elements are arranged in a curvilinear array.
- Phased array probes: the piezoelectric elements are arranged in a rectangular or square matrix.
- Endocavitary probes: these probes are designed for internal imaging, such as transvaginal or transrectal scans.

Additionally, advancements in technology have led to 3D and 4D ultrasound probes, which capture volumetric data. 3D probes construct a three-dimensional image, while 4D ultrasound adds a time dimension, allowing real-time imaging of moving structures, such as a beating fetal heart.

3.4 Visualization mode

There are different strategies for visualizing ultrasound data:

- A-mode (Amplitude mode): This technology involves the use of a single scan line. With this acquisition mode, a signal is obtained—not an image—characterized by a pulse for each discontinuity encountered by the generated acoustic wave. The vertical axis represents the depth of the discontinuity, while the horizontal axis represents the amplitude of the returning echo (Figure 3.2 (a)). Currently, this acquisition strategy is no longer in use.
- B-mode (Brightness mode): This acquisition mode combines a series of scan lines to create the ultrasound image. What is represented is a bright dot at the position where a returning echo was received, with the color proportional to the intensity of the echo (Figure 3.2 (b)). When the received echo is very intense, the color is black; when no echo is received, the color is white.
- M-mode (Time Motion mode): Uses a single scan line which generates a graph in which the motion of each interface along this scan line is plotted as a function of depth and time (Figure 3.2 (b)). Normally, this mode is used together with B-mode, allowing the visualization of point movements over time.

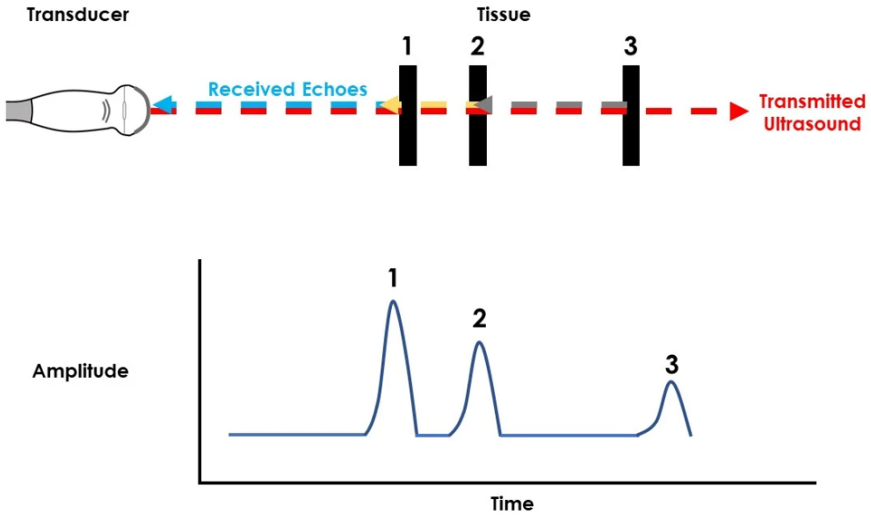

(a) A-mode.

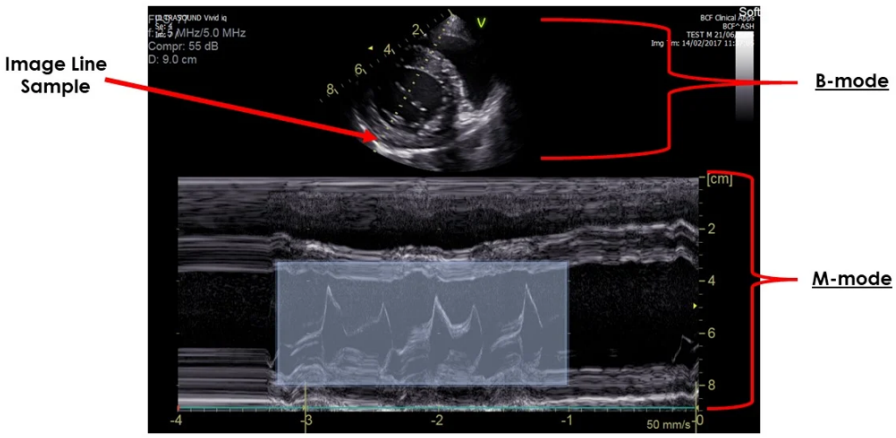

(b) B-mode and M-mode.

Figure 3.2: Different strategies for visualizing ultrasound data [4].

Chapter 4

Fluid therapy

The term fluid therapy is a fundamental therapeutic intervention that includes any form of fluid administration to maintain or restore water and electrolyte balance in the body. It is used in various clinical contexts, from emergency to surgical and intensive care settings and it may include oral, enteral, and intravenous (IV) fluids. Intravenous fluid therapy involves administering fluids directly into the bloodstream through a vein. It is one of the most common therapeutic interventions performed in emergency departments and has long been an established treatment. Most research on fluids has focused on patients with critical illnesses [12].
Intravenous fluid therapy can include different types of fluids: crystalloids (which contain sodium in the range 130154 mmol/L, with a bolus of 500 mL in less than 15 minutes) and colloids (a mixture in which a substance consisting of insoluble particles dispersed microscopically is suspended in another substance) [12]. In particular, the fluid challenge— a specific application of intravenous (IV) therapy— has been proposed for years to guide fluid therapy. It specifically involves the administration of a bolus of 200-500 mL of fluid to evaluate the patient's hemodynamic response. Despite its undeniable benefits, intravenous fluid therapy presents critical issues that can have a negative impact on the patient's health if not managed correctly.
One of the main problems is the risk of fluid overload. Particularly in critically ill patients, excessive fluid administration can lead to serious consequences such as pulmonary edema and congestive heart failure [17]. Furthermore, correctly balancing fluid volume can be a challenge: administering too much fluid can compromise kidney and lung function, while insufficient management may not meet the patient's hemodynamic needs [17]. Another aspect to consider is the variability of patient responses. Not everyone responds the same way to fluid administration, and evaluating their effectiveness requires constant monitoring and in-depth knowledge of the patient's underlying condition [17].
To reduce the invasiveness of the classic fluid challenge, the idea of a "mini-fluid challenge" was born, performed with a rather small volume of fluid to evaluate the reactivity to preload. It consists of infusing, for a period of 60 to 120 seconds, 100 to 150 mL of crystalloid or colloid, and then measuring the response of cardiac output (CO) or one of its surrogates. Several studies in recent years have demonstrated that the mini-fluid challenge reliably predicts response to volume expansion [24]. During a classic fluid test, it is well demonstrated that changes in blood pressure

very loosely follow changes in cardiac output. The same obviously applies to a mini-fluid challenge, during which it is therefore necessary to directly estimate the cardiac output or stroke volume (Figure 4.1) [24].

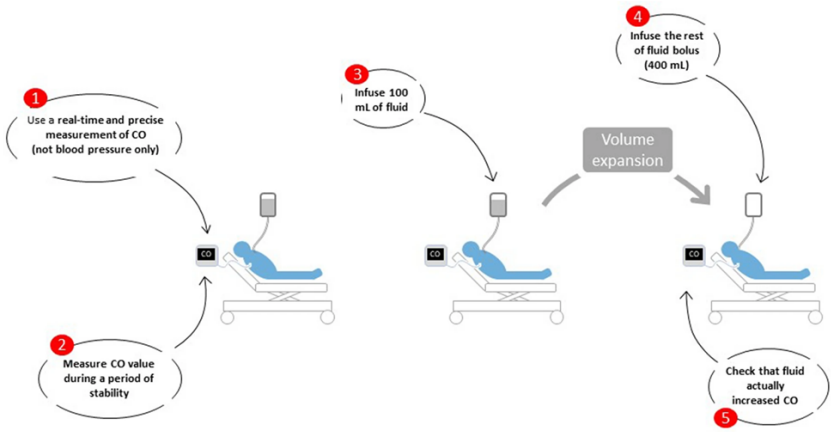

Figure 4.1: Practical rules for performing a mini-fluid challenge. *CO* cardiac output [24].

The mini-fluid challenge, although in smaller quantities, still involves the infusion of fluid which, if ineffective, cannot be removed. Furthermore, if repeated, it too can intrinsically induce fluid overload, although the risk is lower than a classic fluid test [24].
In such a complex context, the need therefore emerges for tools and techniques that can help the clinician make more informed decisions and avoid the risks associated with excessive or incorrect administration of fluids. Passive Leg Raising (PLR) represents a less invasive, but equally effective, alternative for evaluating a patient's ability to respond to fluids. Unlike intravenous fluid therapy, which requires the introduction of liquids into the body with potential risks, PLR is a simple maneuver that allows you to obtain an immediate and dynamic hemodynamic evaluation, simulating the effect of a load of fluids without actually administering them.

4.1 Passive leg raising (PLR)

The passive leg raising (PLR) test is a current method used in functional hemodynamic monitoring to evaluate cardiac preload responsiveness, i.e. the heart's ability to respond to a temporary increase in the volume of blood returning to the heart (preload) [22]. Preload refers to the loading condition of the heart (the amount of blood that fills the ventricles) at the end of diastole, which is the phase of relaxation and filling, just before contraction (systole). It represents the degree of tension in the cardiac fibers at the end of diastole (end-diastolic tension) and the end-diastolic volume, which depends on the ventricular pressure during diastole and the composition of the myocardial wall.
This test simulates a fluid challenge by temporarily shifting blood from the lower

extremities to the central circulatory system without the need for intravenous fluid administration [34]. When a patient's legs are raised passively from the horizontal plane, gravity causes approximately 150-300 mL of blood to move from the venous reservoir in the lower body, especially the calves, toward the central circulation and the heart [9]. In addition, the test does not depend on ventilation and heart rate, and it remains reliable in patients with spontaneous ventilation and cardiac arrhythmia [24]. This natural "fluid loading test" temporarily increases venous return and preload, mimicking the effect of rapid intravenous fluid administration. By observing how the heart responds, healthcare providers can determine if a patient would benefit from fluid therapy [34].

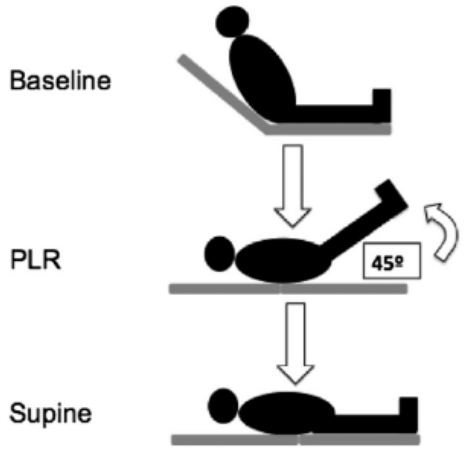

Figure 4.2: Passive leg raising maneuver [20].

This is particularly important in critically ill patients, as administering unnecessary fluids can lead to fluid overload, causing complications such as pulmonary edema or cardiac stress. The PLR test is effective because it temporarily converts unstressed venous volume, which does not contribute to circulatory pressure, into stressed volume, supporting venous return and increasing preload [34]. If the heart responds with an increase in stroke volume (SV) or cardiac output (CO), it indicates that the patient is preload responsive and would likely benefit from additional fluid therapy [18]. The reliability of the PLR test regarding the detection of reactivity to preload is consolidated. The test, in addition to good sensitivity and specificity (85 and 91% respectively), also has positive and negative predictive values and very good likelihood ratios [24].
According to Monnet and Teboul, there are five key rules to consider when performing a PLR test [23]. First, the PLR should begin from a semi-recumbent position rather than a supine position (Figure 4.2). Second, the effects of PLR should be evaluated through direct measurement of cardiac output, not just blood pressure. Third, the method used to measure cardiac output during PLR should detect short-term and transient changes, as the effects of PLR can disappear within a minute. Fourth, cardiac output should be measured not only before and during PLR but

also after, to ensure it returns to baseline. Finally, factors like pain, coughing, discomfort, or awakening can trigger adrenergic stimulation, potentially leading to incorrect interpretations of changes in cardiac output [23].
The ways to measure cardiac output during PLR can be different. The volume clamp technique estimates cardiac output through the uncalibrated analysis of an arterial curve obtained noninvasively through a finger cuff. Echocardiography and esophageal Doppler, which estimate the stroke volume beat by beat, are also very suitable. it is also possible to proceed with cardiac ultrasound, but to guarantee the precision of the measurement, it is advisable to keep the probe on the patient's skin and the ultrasound beam in the outflow tract of the left ventricle (LVOT). In ventilated patients without spontaneous respiratory activity, changes in carbon dioxide measured at the end of expiration at the tip of the tracheal tube can provide information about changes in cardiac output. This approach allows monitoring the effects of the fluid load response (PLR) test, representing an interesting alternative to traditional methods, especially during surgical interventions and under anesthesia [24].

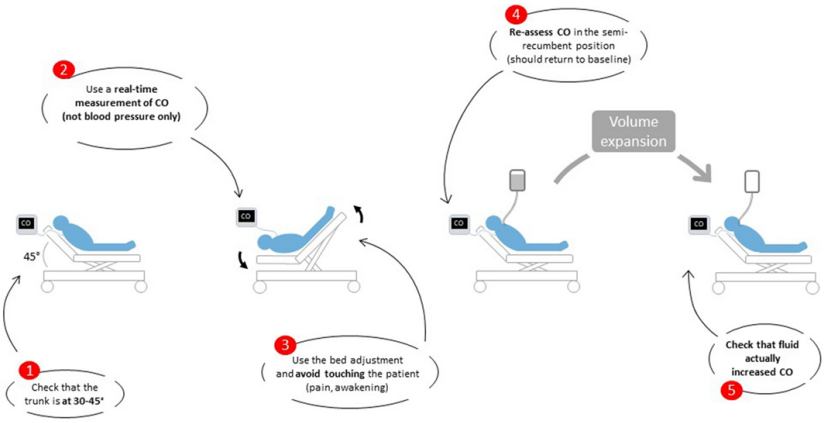

Figure 4.3: Practical rules for performing passive leg raising. *CO* cardiac output [24]

4.2 Hemodynamic Monitoring in Fluid Therapies

In the context of fluid therapy, monitoring the patient's hemodynamic status is essential to ensure effective treatment. Pulsatility indices, such as caval index (CI), collapsibility index (CCI), and respiratory collapsibility index (RCI), provide crucial data on the size and responsiveness of the inferior vena cava (IVC) during maneuvers such as passive leg raising (PLR). These indices not only help assess the patient's ability to tolerate increased blood volume, but can also guide clinical decisions regarding appropriate fluid administration, thereby optimizing therapy.

4.2.1 Caval index (CI)

The diameter of the inferior vena cava (IVC) varies with the respiratory cycle. During inspiration, the negative pressure generated favors a greater return of blood to the heart, causing a temporary collapse of the IVC. On the contrary, during exhalation, venous return is reduced, allowing the vena cava to restore its original diameter [39]. The percentage of variation in the diameter of the IVC during breathing, called the collapsibility index, can be used to evaluate the state of the intravascular volume and the pressure of the right heart, proving particularly useful in the management of resuscitation, especially in cases of non-specific hypotension or shock [39]. In fact, through ultrasound it is possible to measure the diameters of the IVC both during inspiration and expiration. These measurements allow the calculation of the collapsibility index, also known as Caval Index (CI), which in turn offers an estimate of central venous pressure (CVP) [39].
The Caval Index also allows the pulsatility of the vena cava to be assessed, from which the mechanical characteristics of the blood vessels can be deduced [10]. It is calculated as:

$$CI = \left(\frac{D_{\max} - D_{\min}}{D_{\max}} \right) \tag{4.2.1}$$

where $D_{\max}$ is the maximum diameter at the end of the expiratory phase and $D_{\min}$ is the minimum diameter at the end of the inspiratory phase [10].
Dynamic parameters reflect heart-lung interactions and vary with cardiac and respiratory cycles. In particular, Caval Index (CI) values are frequently used to evaluate the state of venous filling and the variability of the diameter of the inferior vena cava (IVC) during the respiratory cycle [15]. In general, lower CI values indicate greater hemodynamic stability, while higher values may be associated with greater variability and therefore a potential reduced preload state or hypovolemic conditions. Cyclic variation of any dynamic parameter is more pronounced in volume-supported patients, making dynamic parameters more reliable than static parameters in predicting volume responsiveness. Accurately predicting volume responsiveness can help avoid volume overload and acute pulmonary edema, or inadequate volume reproduction [15].
In the clinical context, a low CI (values closer to 0) indicates that the IVC is less compressible and varies little during the respiratory cycle. This may be a sign of a more stable and adequate blood volume. In particular, in healthy subjects, such as the subjects examined during this thesis work, a lower CI suggests that the cardiovascular system is well filled and that there is less variability in venous blood flow. A high CI (values closer to 1), however, indicates that the IVC is very compressible, with significant variations between inspiration and expiration. This may suggest that the subject is more susceptible to changes in preload, potentially due to decreased hemodynamic stability or hypovolemia. This index, however, is subject to great variability, which translates into low reliability.
Over the years, thanks to the development of new algorithms, techniques have been developed capable of compensating some of the effects that caused variability, improving the repeatability of measurements. However, factors such as the intrinsic variability of spontaneous activity respiratory activity represent a large source of variability in the breath-phase oscillation of IVC dimensions [10].

An innovative approach to studying the dimensions of the inferior vena cava (IVC) consists of automatic video analysis and offers a continuous view of changes in these dimensions, allowing for the independent separation and analysis of the influences of the heartbeat and respiration. Two additional indices are introduced: the cardiac caval index (CCI) and the respiratory caval index (RCI) [10]. In particular, the CCI accounts of the IVC cardiac variation, the RCI is defined as the percentage decrease in the diameter of the IVC at the end of the inspiratory phase [19].

Chapter 5

Methods

5.1 IVC segmentation

In clinical diagnosis and surgical planning, the segmentation of the inferior vena cava (IVC) is crucial because it significantly impacts both the accuracy of liver volumetry and the analysis of vascularization [16]. It has various medical applications, including liver health assessment, evaluation of hydration status and hemodynamic load, oncology, computer-assisted surgery, and advanced imaging technologies. However, this process faces several challenges:

- Anatomical variability: The IVC can exhibit morphological differences between patients, complicating the development of universally applicable segmentation models [14].
- Lack of clear boundaries: In medical imaging, the boundaries between the IVC and surrounding tissues, such as the liver and nearby blood vessels, are often indistinct. This makes it difficult to isolate the IVC accurately in modalities like MRI, CT, or ultrasound [16].
- Complexity of surrounding structures: The IVC is located in a complex anatomical region, surrounded by vascular and tissue structures, such as the hepatic veins, further complicating the segmentation process. Advanced segmentation techniques, including machine learning algorithms and active contour models, are needed to address these challenges [16].

As a result, accurate IVC segmentation remains an ongoing challenge, despite technological advancements, due to these anatomical and imaging-related complexities.

5.2 VIPER

Ultrasound of the inferior vena cava (IVC) provides important information on the patient's clinical status, particularly regarding fluid volume and RAP; this allows to support healthcare workers in the diagnosis and effective monitoring of patients [40]. Evaluating the diameter and pulsatility of the IVC in a standard manner can be

difficult due to three main problems: its irregular shape, the movement caused by breathing and cardiac activity, and the variability in measurements due to differences between operators or even between measurements carried out by the same operator.
To address these challenges, a semi-automatic tracking algorithm called VIPER was developed in Matlab. This algorithm allows detailed analysis of the IVC along both the longitudinal and transverse axes. By constantly tracking the same sections of the vein and compensating for movements, VIPER processes the ultrasound images providing real-time output. This software offers more accurate and reliable measurements providing practical benefits to the healthcare professional [40].

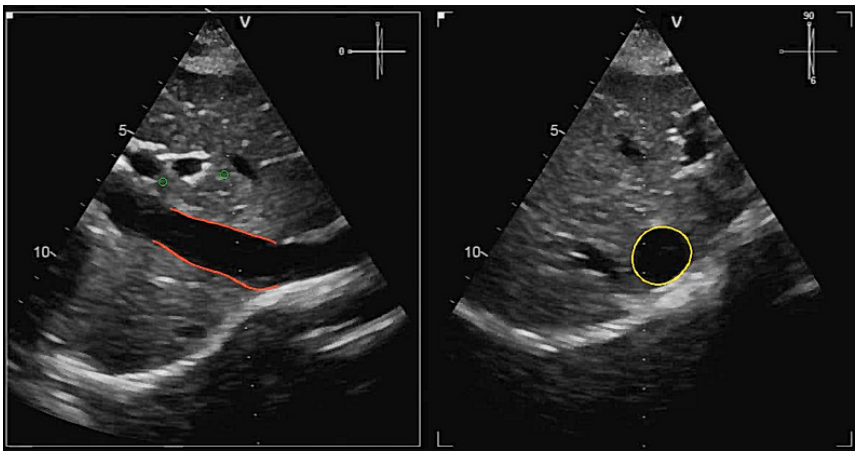

Figure 5.1: Example of a frame from an ultrasound video clip where the IVC is correctly segmented, via the software, along the longitudinal axis (left) and the transverse axis (right) [40].

5.2.1 Segmentation software

For this work, the segmentation of the vena cava was carried out using the VIPER software. This software is based on an algorithm that requires as input the video clip of the ultrasound of the inferior vena cava, in longitudinal or transversal section. The algorithm allows each frame of the ultrasound to be processed, generating the upper and lower edges of the vein, i.e. segmenting it. When the video clip is provided as input, the algorithm asks the operator to select two reference points which are used to follow the movements of the inferior vena cava throughout the duration of the analysis (Figure 5.2).

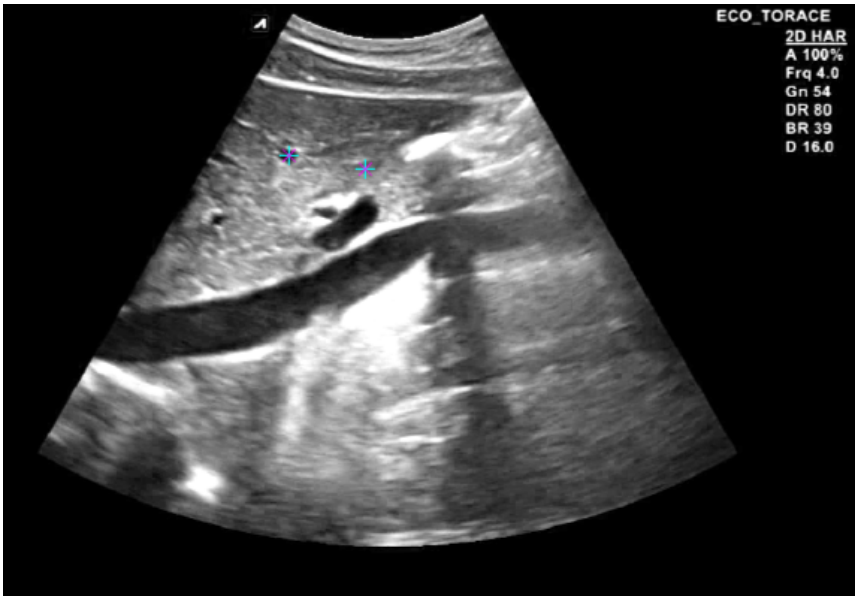

Figure 5.2: Manual selection of two reference points.

Once the reference points have been selected, the operator must select a point on the upper edge and one on the lower edge of the vein, i.e. he must identify the diameter of the vein from which to start the analysis (Figure 5.3).

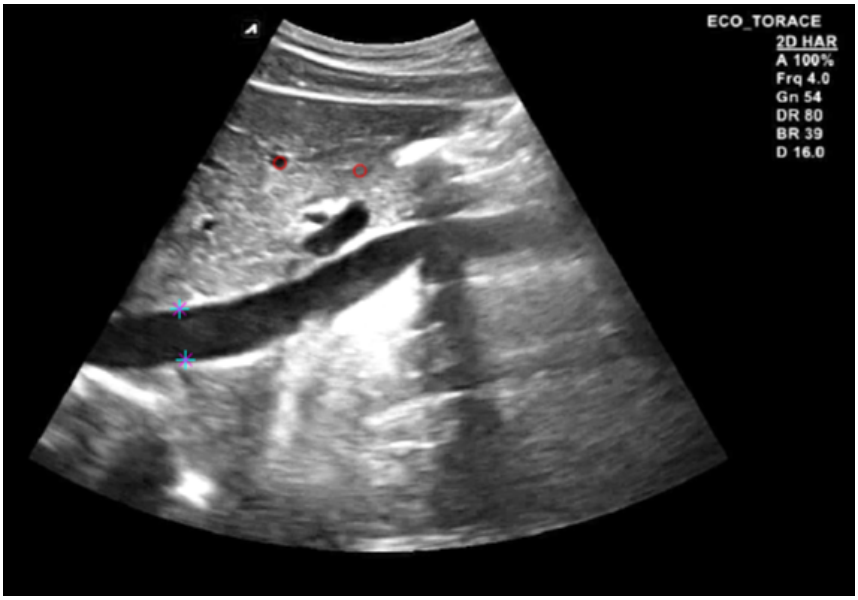

Figure 5.3: Selection of one point on the upper and one on the lower edge of the vein.

Finally, the operator draws a segment on the right end of the vein which indicates the terminal part of the vein to be segmented (Figure 5.4).

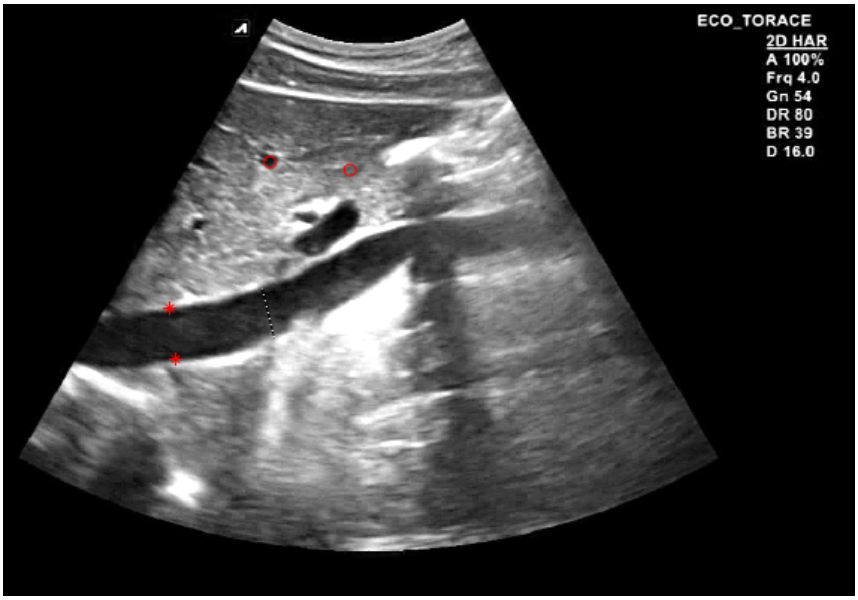

Figure 5.4: Drawing the segment on the right end of the vein.

Once the IVC is segmented, the diameters are calculated. The algorithm determines the midline of the vein, calculated as the average of the upper and lower edges of each ultrasound frame. The midline is then interpolated with a parabola, and its total length is calculated. Subsequently, 5 % of the length is excluded at both the upstream and downstream ends, eliminating the extremities. On this new length, 21 points are uniformly distributed, and for each point, a line perpendicular to the midline and passing through the considered point is drawn. The diameter of the vein is defined as the intersection between this new line and the two edges of the vein. This process yields 21 diameters for each frame; these 21 diameters are then averaged to obtain a single diameter value for each frame.

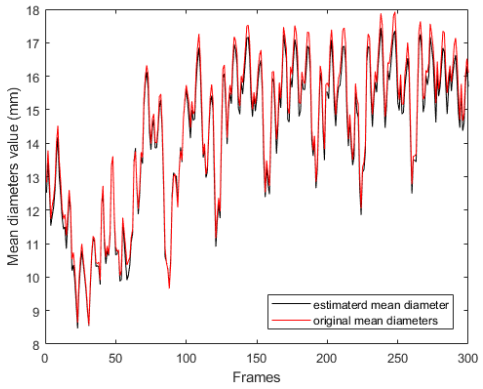

(a) The x-axis shows the frames of the ultrasound video clip, the y-axis the values of the mean diameters (average of the 21 diameters per frame) in millimeters for each frame. This results in a graph showing the trend of the estimated mean diameter values and the original mean diameters for each frame of the analyzed video clip. For better visualization, the signal is shown limited to 300 frames of 1861.

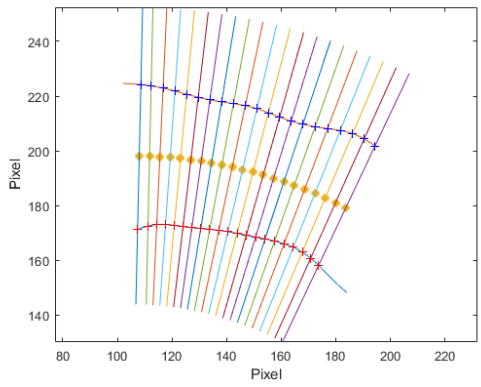

(b) The yellow points represent the uniform distribution of 21 points in the portion of the vein between 5 % and 95 % of its total length. For each of the 21 points, a perpendicular is drawn passing through the midline and through the point itself; the intersections of the perpendicular with the upper and lower edge (blue and red line) determine the diameter.

Figure 5.5: Calculation of mean diameters for each frame.

The next phase of the analysis is the extraction of pulsatility parameters. However, to perform this analysis, it is necessary to convert the unit of measurement of the diameters from pixels to millimeters. The conversion is done by multiplying the diameter value in pixels by a conversion coefficient calculated based on the scan depth of the ultrasound video.

5.2.2 Parameter extraction

Once the mean diameter values for each frame are obtained, it is possible to identify the maximum and minimum diameter values and then calculate the pulsatility index or caval index using formula (4.2.1). Considering that the changes in the IVC diameter are determined by two distinct components—cardiac and respiratory—it is possible to isolate each components to also calculate the cardiac caval index (CCI) and the respiratory caval index (RCI), by applying the same formula exclusively to the respective component.

5.3 Descriptive statistics

Descriptive statistics is a key area of statistics focused on summarizing and presenting the essential characteristics of a dataset. It provides tools for organizing, visualizing, and interpreting data in a straightforward manner, without making inferences or predictions beyond the data itself. Key components of descriptive statistics

include measures of central tendency, such as the mean, median, and mode, which indicate the typical value within the dataset. Additionally, measures of dispersion, like range, variance, and standard deviation, describe the variability or spread of the data. Frequency distributions, often represented through histograms or frequency tables, and graphical tools like box plots, bar charts, and pie charts, are also commonly used.
Together, these techniques offer a clear and concise overview of the data, making it easier to interpret and understand its structure.

5.3.1 Boxplot

Box plots are graphical tools used to display the distribution of numerical data, particularly useful for comparing distributions across multiple groups. They provide a concise summary of the data, highlighting key features such as symmetry, skewness, variability, and the presence of outliers.
Box plots make it easy to identify the central portion of the data and compare these characteristics across different groups. By visually summarizing range and distribution patterns, they provide a clear view of how different data sets compare, allowing you to quickly and easily spot trends and overall differences. A box plot illustrates the distribution of a set of numerical data using five indices:

- Minimum: The lowest value (excluding any outliers).
- First quartile (Q1): The 25th percentile, the value below which 25 % of the data falls.
- Median (Q2): The 50th percentile, dividing the data into two halves. It is located in the middle of the "box" and represents the median value of the distribution.
- Third quartile (Q3): The 75th percentile, the value below which 75 % of the data falls.
- Maximum: The highest value (excluding any outliers).

The "box" of the box plot extends from the first quartile (Q1) to the third quartile (Q3), and the distance between Q1 and Q3 is called the interquartile range (IQR). The "whiskers" (lines) extend from the box to the minimum and maximum values, unless there are outliers, which are displayed as isolated points outside the whiskers. Outliers are typically defined as values that fall more than 1.5 times the IQR beyond the first and third quartiles and they are plotted individually using the `'+'` marker symbol [5].

5.3.2 Coefficient of variation (CV)

The coefficient of variation is a descriptive numerical indicator that provides information on the variability of a quantitative variable. In particular, it is a measure of relative variability and provides a dimensionless value, as it does not depend on

the unit of measurement or the size of the variable under examination. The CV is calculated as follows:

$$CV = \frac{\sigma}{\mu} \times 100\ \% \tag{5.3.1}$$

where σ is the standard deviation and μ is the mean value of the data distribution. The CV is always a positive value or zero, as both the standard deviation and the mean are non-negative values. It allows for the comparison of the dispersion of two or more datasets, even if they have different scales or units of measurement. A low CV indicates that the standard deviation is relatively small compared to the mean, meaning the data are more homogeneous and tend to be close to the mean. A high CV indicates that the standard deviation is large relative to the mean, meaning the data are more dispersed, which implies that there are greater differences between the values.

5.4 Inferential statistics

Inferential statistics is a branch of statistics that focuses on making predictions and generalizing about a larger population based on sample data. By analyzing the sample, it is possible to extend the results to the population without having to directly study each individual in it.
The key methods in inferential statistics are divided into parametric and non-parametric. Parametric tests are used when the data under examination follow a normal distribution, have the same variance and are randomly drawn from the population. Non-parametric tests, on the other hand, do not assume a normal distribution of the data. In general, they are used for small samples, for data that, in fact, do not follow a normal distribution and are not sensitive to outliers like parametric tests.
In this thesis, parametric methods will be used for data that follow a normal distribution and non-parametric tests for data that significantly deviate from normality.

5.4.1 Two-way analysis of variance (ANOVA)

Two-way analysis of variance (ANOVA) is a variant of analysis of variance (ANOVA) [13]. ANOVA is a parametric statistical analysis method that can split an aggregate variability observed within a data set into two parts: the variability due to systematic factors and that due to random factors. While systematic factors influence the data set, random factors do not. ANOVA allows you to make comparisons between three or more groups of data, a tool that can identify the factors that influence a given result [13].
Two-way ANOVA compares the mean differences between groups of data that have been divided into two independent variables (factors). It is a statistical test useful for determining the effect of two independent variables on a single dependent variable. Specifically, two-way ANOVA examines the main effect that each of the two independent variables has on the expected result, allowing you to determine whether the variability of the results is due to the factors in the analysis or to random factors [13].

5.4.2 Paired sample t-test

The Student t-test (t-test) is a statistical tool for analyzing the means of one or two populations by testing hypotheses. A t-test can be used to examine whether a single group differs from a known value (a one-sample t-test), whether two groups differ from each other (a two-independent-sample t-test), or whether there is a significant difference in paired measurements (a paired-sample t-test) [36].
The paired-samples t-test compares the means of two measurements taken on the same individual or related units. The purpose of the test is to determine whether there is statistical evidence that the mean difference between paired observations is significantly different from zero. The paired-samples t-test is a parametric statistical test that is designed to determine whether there is statistical evidence that the mean difference between paired observations is statistically different from zero [35]. Paired measurements can be represented as measurements taken at two different times or under two different conditions [35].
The test statistic for the paired-samples t-test follows the same formula as the one-sample t-test:

$$t = \frac{\bar{d}}{\frac{s_d}{\sqrt{n}}} \tag{5.4.1}$$

where, n is the number of observations, s_d is the standard deviation of the differences and $\bar{d}$ is the mean of the differences between pairs of observations, calculated as:

$$\bar{d} = \frac{1}{n}\sum_{i=1}^{n} d_i \tag{5.4.2}$$

where $d_i = X_1 i - X_2 i$, i.e. the difference between the two measurements for each subject i. In the (5.4.1) formula, s_d is calculated as follow:

$$s_d = \sqrt{\frac{1}{n-1}\sum_{i=1}^{n}(d_i - \bar{d})^2} \tag{5.4.3}$$

The calculated t-value reflects the magnitude of the observed mean difference relative to the variation in individual differences. Once calculated, it is compared to a reference value, called the critical t-value, which depends on the number of samples with degrees of freedom $df = n-1$ and the chosen confidence level. If the calculated t-value is greater than the critical t-value, it means that the test has observed a significant difference between the means, that is, the null hypothesis is rejected, which states that there are no significant differences between the two measurement times. If the calculated t-value is less than the critical t-value, there is not enough evidence to state that the two means are significantly different, so the null hypothesis cannot be rejected.

5.4.3 Wilcoxon signed rank test

The Wilcoxon signed-rank test is a non-parametric method utilized to compare two related samples and is the nonparametric alternative to the Student t-test [32]. It

considers information about the sign and magnitude of differences between pairs of samples. It is considered the most valid signed test because it considers a large amount of information about the data being analyzed. The formula for calculating the Wilcoxon T-test is as follows:

$$T = \text{smaller of } \sum R^{+} \text{ and } \sum R^{-} \tag{5.4.4}$$

where R^{+} is the ranks for the positive differences and R^{-} is the ranks for the negative differences. Once the T statistic is calculated, it is compared to a critical value, determined based on the chosen significance level and the number of pairs of observations. If the calculated T is less than or equal to the critical value, the null hypothesis is rejected, that is, it is established that there are significant differences between the paired samples. On the contrary, if the calculated T is greater than the critical value, there is not enough evidence to reject the null hypothesis, suggesting that there is not enough evidence to conclude that there are significant differences between the paired samples.

Chapter 6

Results and discussion

The main objective of this study is to evaluate the effect of the passive leg raising (PLR) maneuver on the inferior vena cava (IVC) in a group of thirteen healthy subjects (5 men and 8 women) with a mean age of 27 ± 9.5 years. The inferior vena cava was chosen for the analysis due to its ability to act as an indicator of venous filling and as a predictor of hemodynamic variability.
For this work, ultrasound videos of the IVC, recorded during two successive PLR maneuvers and belonging to the subjects under examination, were processed using the software developed by VIPER s.r.l.. The ultrasound processing was aimed at segmenting the inferior vena cava (IVC) with subsequent calculation of hemodynamic parameters of clinical interest, such as the mean diameter of the IVC and pulsatility indices. These parameters provide information on blood volume variations, proving to be fundamental for understanding the patient's circulatory response to PLR.
For the purposes of analysis, each PLR maneuver was divided into three key measurement moments: before (baseline), during and immediately after the maneuver. Therefore, for each subject, the mean IVC diameters and pulsatility indices, such as CI, CCI and RCI, were calculated in six key time states.
A mean interval of 23.82 ± 3.47 minutes was maintained between the two PLR maneuvers, in line with the literature indications, which suggest a minimum pause of 5-10 minutes to restore hemodynamic homeostasis. As for the two maneuvers themselves, however, they were performed and maintained for at least two minutes, always in line with the indications in the literature, which indicate that it is necessary to maintain the PLR for at least 1-2 minutes since the maximum effect of the maneuver occurs 30-90 seconds after the start of the maneuver itself [25].
For a first assessment of the effect of the PLR maneuver on the hemodynamic response of the IVC, the trends of the mean IVC diameter and pulsatility index (CI) were visualized in the six time states of interest. In particular, during the PLR maneuvers, compared to baseline and post maneuver, the IVC diameter was expected to increase, while the caval index (CI) did not. This is because the PLR maneuver temporarily increases venous return to the heart, as leg elevation facilitates the movement of blood from the lower limbs toward the central circulation. This additional blood flow to the IVC causes a temporary increase in its diameter. In fact, the IVC diameter is often used as a marker of central venous pressure: when venous return increases, as occurs in PLR, the IVC diameter tends to increase proportion-

ally to the amount of additional blood that is passing at that moment. In contrast, CI measures the variability of blood flow within the IVC, which will be greater when there is little venous return and less when there is increased venous return, such as during PLR, which stabilizes and regulates blood flow.
The significant changes in mean diameters and CI between baseline, during PLR and post-maneuver phases are illustrated below. For the sake of synthesis, representative results from two subjects out of the 13 analyzed are presented. The analyses for all subjects belonging to the considered dataset are reported in the appendix A.

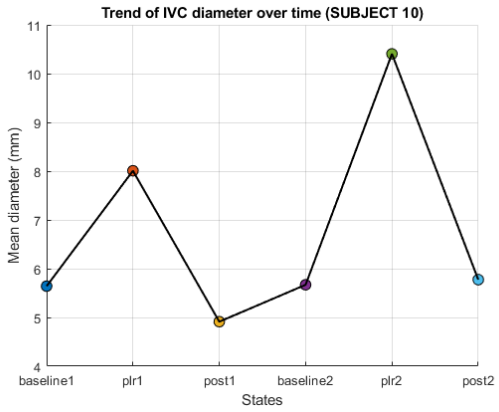

(a) Trend of mean diameter values of subject 10 during baseline, PLR and post-maneuvers for both PLR maneuvers.

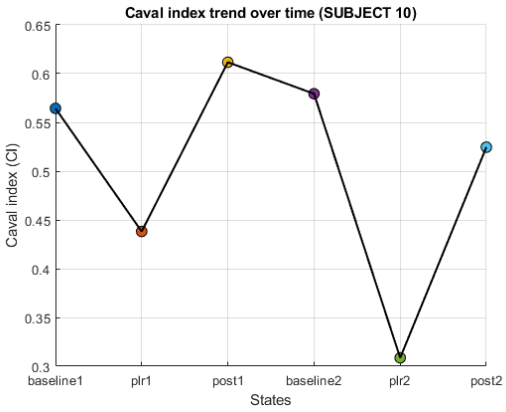

(b) Trend of CI values of subject 10 during baseline, PLR and post-maneuvers for both PLR maneuvers.

Figure 6.1: Trend of the mean IVC diameter and pulsatility index (CI) over the time of the subject 10.

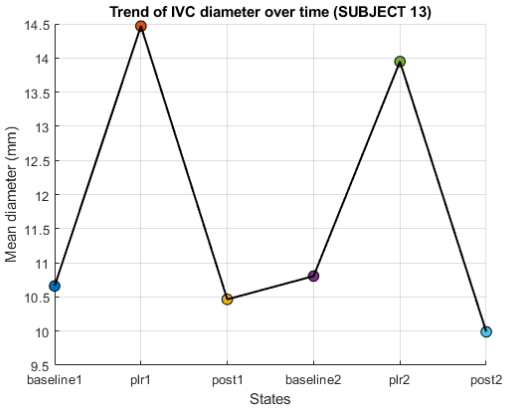

(a) Trend of mean diameter values of subject 13 during baseline, PLR and post-maneuvers for both PLR maneuvers.

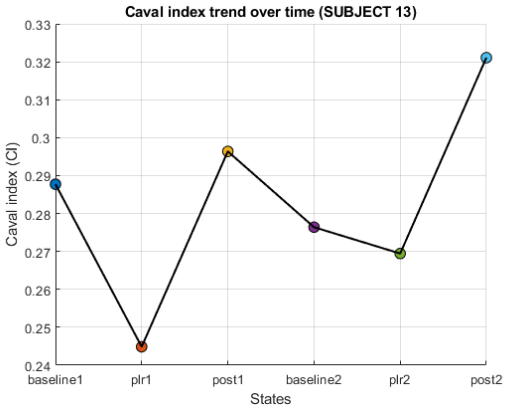

(b) Trend of CI values of subject 13 during baseline, PLR and post-maneuvers for both PLR maneuvers.

Figure 6.2: Trend of the mean IVC diameter and pulsatility index (CI) over the time of the subject 13.

To provide a clearer view and immediate information on individual trends compared to the average behavior, a line graph was created that shows the trend of the average diameter and the CI during the transition from the baseline to the PLR maneuver, for both maneuvers. All values were normalized with respect to the baseline value in order to be able to view the trend of each parameter starting from a null value, thus immediately highlighting the increasing and decreasing trends. In this way, it is easier to identify the subjects who present trends that deviate from the general trend. This representation also helps to easily identify any atypical or individual responses to the PLR and to better understand the variability between the subjects under examination.

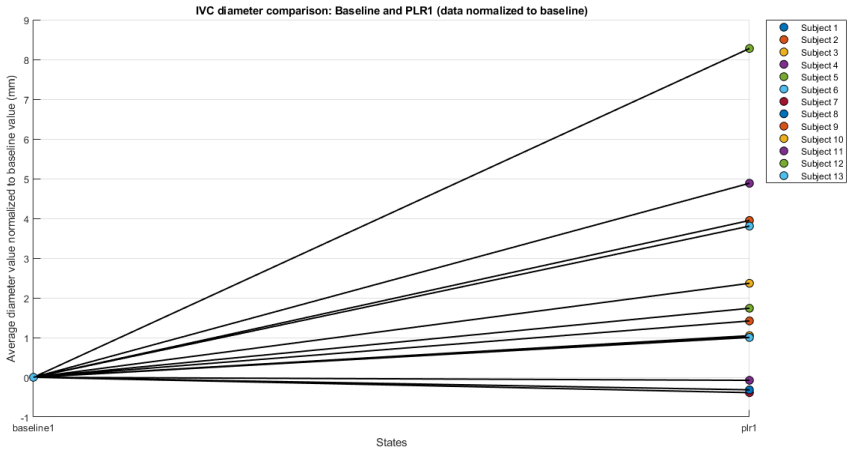

(a) Mean diameter trend during the transition from baseline to the first PLR maneuver.

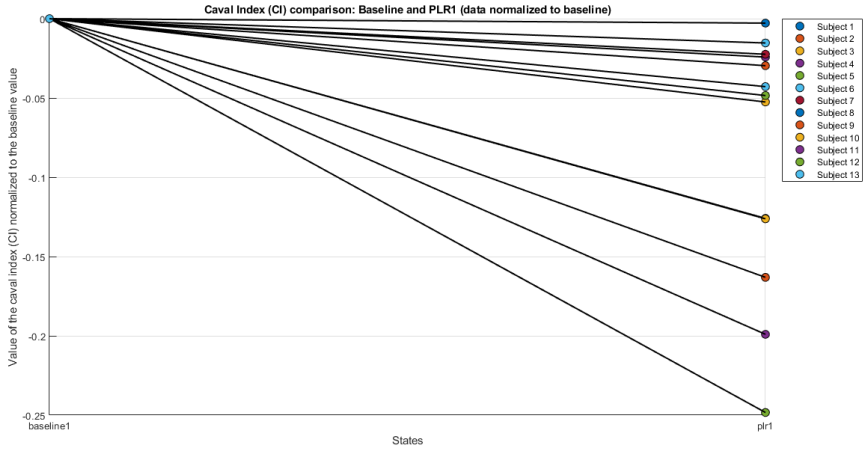

(b) CI trend during the transition from baseline to the first PLR maneuver.

Figure 6.3: Trend of the mean IVC diameter and caval index (CI) during the transition from baseline to the first PLR maneuver.

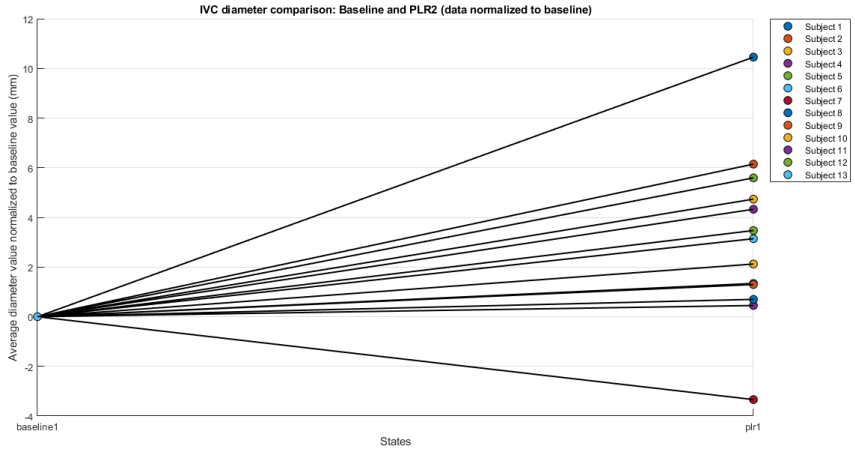

(a) Mean diameter trend during the transition from baseline to the second PLR maneuver.

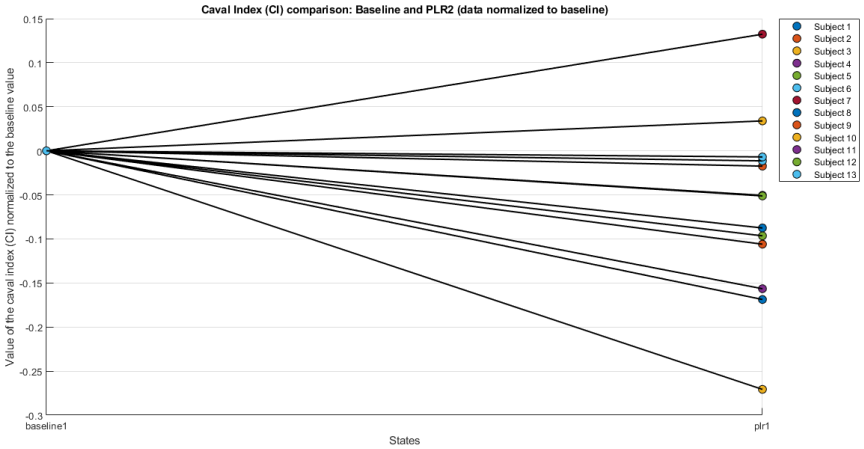

(b) CI trend during the transition from baseline to the second PLR maneuver.

Figure 6.4: Trend of the mean IVC diameter and caval index (CI) during the transition from baseline to the second PLR maneuver.

These data show how some subjects are characterized by trends in hemodynamic parameters that do not follow the general trend of the sample. These anomalous results could be related to the quality of the ultrasound recordings. In ultrasound images, in fact, small variations in position or technical difficulties in visualizing the IVC can affect the accuracy of the measurements of the mean diameters, and consequently also of the pulsatility indices, leading to variations that are not necessarily representative of the real hemodynamic state of the subject.
Once the consistency of the trends of the indices and diameters observed between the subjects was assessed, the next step of this study was to analyze the data with statistical methods to determine the actual significance of the hemodynamic changes before, during and after the two PLR maneuvers. This step allows us to understand whether the variations in the diameters and pulsatility indices of the IVC reflect a systematic adaptation of the body to the maneuver. In order to obtain a gen-

eral view of the data distribution, they were first studied using descriptive statistics methods. In particular, boxplots and coefficient of variation (CV) were used:

- Boxplots were used to visualize the distribution of pulsatility indices (CI, CCI, RCI) and relative diameters during each temporal state for each subject. This graphical representation allowed us to quickly identify the median, variability, presence of outliers, and differences between the two maneuvers for each index.

- The CV was calculated for each pulsatility index and for the mean diameters, in order to evaluate the relative variability between the parameters. This indicator allowed to understand how much the values of each parameter varied with respect to their mean, providing information on the homogeneity of the data.

Subsequently, the data were analyzed using inferential statistical methods to assess the significance of the observed differences. In particular, three types of statistical tests were applied: two-way ANOVA for repeated measures, paired samples t-test and Wilcoxon signed-rank test for paired data.

- The two-way ANOVA for repeated measures was used with the aim of evaluating whether the effect of the variability of the temporal states of acquisition and the variability between subjects is significant on the parameters CI, CCI, RCI and mean diameters of the IVC. This test is suitable for data that follow a normal distribution and, in particular, it allows for any significant differences in parameter values not only between the different temporal states of interest, but also between subjects, thus isolating the effects attributable to single physiological variations compared to those due to the PLR maneuver.

- The paired samples t-test was used to compare pairs of temporal states of interest, such as baseline and PLR. This test is suitable for data that follow a normal distribution and allows to compare the means of two time states, to understand if the difference observed between the measurements taken at the two different times depends on the maneuver performed or on the natural variability of the sample.

- The Wilcoxon test for paired data was instead used to evaluate if the mean diameters varied differently in the transition between baseline and PLR between the two maneuvers. The distribution of the variation of the mean diameters between baseline and PLR did not follow a normal distribution, which is why this non-parametric method was applied, which allowed to verify the presence or absence of significantly statistical differences between the two variations.

The choice of these tests was motivated by the need to compare repeated measures within each subject, as well as to explore possible correlations between parameters. The overall approach allowed us to obtain an accurate and robust analysis, considering the characteristics of the data and the assumptions required by the statistical tests used. The statistical analysis was conducted using the MATLAB programming language.

6.1 Descriptive analysis

The boxplots allow to immediately observe a difference in the distribution of data between the various temporal states, confirming how the hemodynamic parameters vary significantly in response to the different phases of analysis. In particular, it is observed how during the execution of the PLR maneuvers, the data relating to the CI, CCI, RCI indices (Figures 6.5, 6.6, 6.7) and the mean diameters (Figure 6.8) are distributed differently compared to the baseline, above all they show a lower variability during the maneuvers. Furthermore, in line with the trends already emerged from the previous graphs, a decrease in the median of the CI is observed during the PLR maneuvers compared to the baselines, which is contrasted by an increase in the median of the mean diameter during the same.

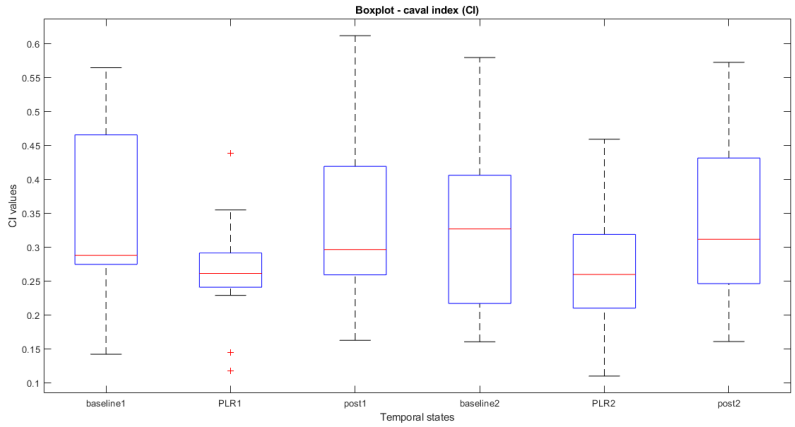

Figure 6.5: Boxplot of all subjects CI values for each temporale state of interest.

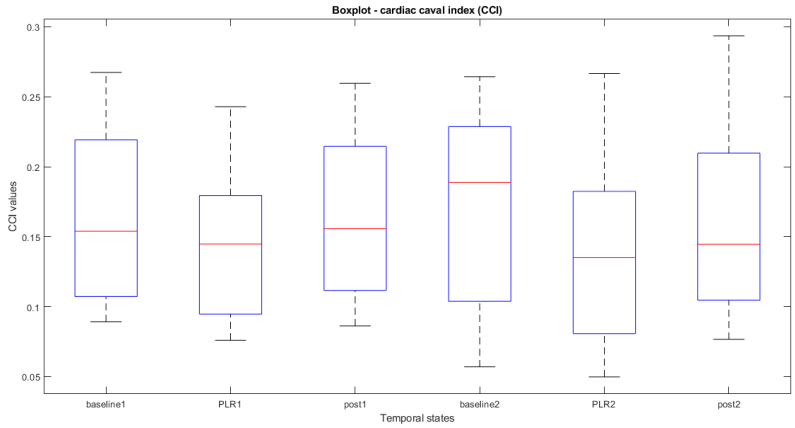

Figure 6.6: Boxplot of all subjects CCI values for each temporale state of interest.

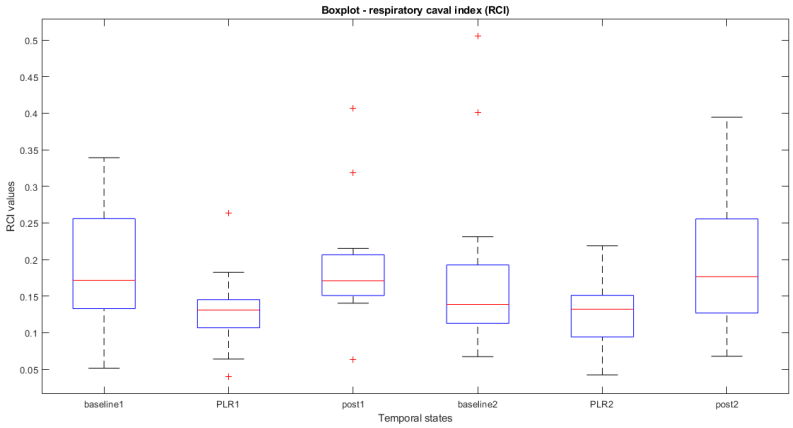

Figure 6.7: Boxplot of all subjects RCI values for each temporale state of interest.

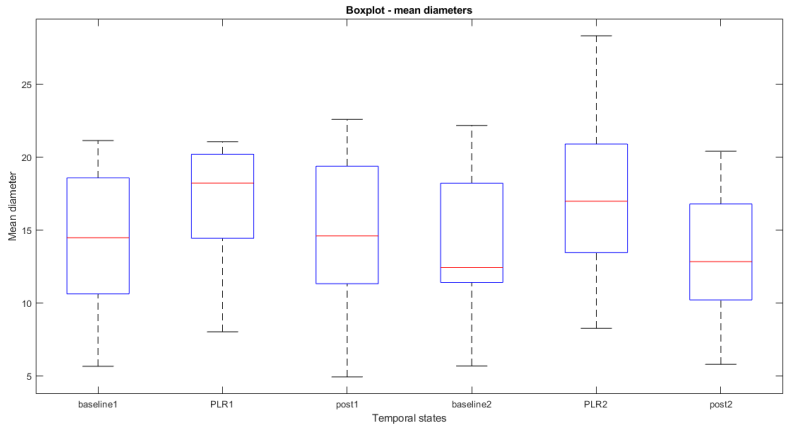

Figure 6.8: Boxplot of mean diameter values for all subjects for each temporal state of interest.

The observations regarding the distribution of the data can also be confirmed by the analysis of the coefficients of variation (CV) calculated for all the pulsatility indices and for all the temporal states of interest. In particular, the table 6.1 highlights how the variation of the CI remains quite stable between the various temporal states, with a decrease during the PLR maneuvers, as shown by the boxplots.
The CV values related to the CCI show a similar trend but with greater variability, especially during and immediately after the second maneuver. This suggests that this parameter could become more sensitive to variations in individual hemodynamic responses for repeated maneuvers.
The RCI shows the highest CV values, especially during the beginning of the second maneuver and during the maneuver itself. The greater variability may be linked to the greater sensitivity of this parameter.

	Baseline1	PLR1	Post1	Baseline2	PLR2	Post2
CI	38.53	30.59	37.26	40.12	37.91	38.98
CCI	37.95	36.21	37.37	41.25	46.90	40.57
RCI	47.09	41.23	44.42	70.05	40.81	51.00

Table 6.1: Coefficient of variation values for all pulsatility indices related to each of the temporal states.

6.2 Inferential analysis

The inferential analysis allowed to study the differences between the parameters under examination and to verify whether these differences were statistically significant. A first analysis was carried out through the ANOVA statistical analysis method, in particular a two-way ANOVA for repeated measures was carried out which allowed to investigate whether there were significant differences between the pulsatility indices and the mean diameters calculated for each time instant and for each subject. The factors that were therefore hypothesized to influence the values of the parameters were two, the different temporal states and the subjects, that is, it was investigated whether there was variability due to the measurements carried out at different time moments and intra-subject variability.
The first step in carrying out this analysis was to organize the data in MATLAB in tables containing all the values of all the parameters for each temporal state and for each subject belonging to the dataset (Tables 6.2, 6.3, 6.4 and 6.5). These tables allowed us to make the data management effective for the two-way ANOVA for repeated measures. Each table contains all the variables of interest, including the levels of the factors and the measures associated with each level. Each column represents the different temporal states, each row a subject.

Subject	Baseline1	PLR1	Post1	Baseline2	PLR2	Post2
1	0.2836	0.2808	0.2794	0.5173	0.3485	0.5723
2	0.2755	0.2459	0.2281	0.1716	0.1542	0.2594
3	0.2813	0.2288	0.2565	0.2099	0.2439	0.2274
4	0.1419	0.1177	0.1626	0.1603	0.1097	0.1607
5	0.5495	0.3012	0.3599	0.3520	0.3008	0.4002
6	0.2715	0.2562	0.2598	0.2565	0.2451	0.2748
7	0.3104	0.2879	0.4172	0.3267	0.4590	0.3115
8	0.4807	0.3548	0.5363	0.4688	0.3813	0.5561
9	0.4399	0.2767	0.3552	0.3654	0.2595	0.2505
10	0.5644	0.4381	0.6117	0.5793	0.3086	0.5246
11	0.4603	0.2612	0.4243	0.3850	0.2285	0.3868
12	0.1932	0.1447	0.2613	0.2192	0.1227	0.2331
13	0.2877	0.2449	0.2964	0.2764	0.2694	0.3211

Table 6.2: CI values for each subject for each time state.

Subject	Baseline1	PLR1	Post1	Baseline2	PLR2	Post2
1	0.1418	0.1395	0.1324	0.1887	0.1349	0.1146
2	0.1211	0.1003	0.0919	0.0570	0.0497	0.1074
3	0.1033	0.0953	0.1221	0.1232	0.1239	0.0767
4	0.0949	0.0753	0.1032	0.0975	0.0768	0.0934
5	0.2674	0.1791	0.1780	0.2251	0.1804	0.2168
6	0.0892	0.0930	0.0862	0.0858	0.0820	0.0966
7	0.2106	0.1804	0.2084	0.2052	0.2665	0.1960
8	0.2097	0.2428	0.2330	0.2644	0.2494	0.2936
9	0.1961	0.1481	0.2009	0.2568	0.1884	0.1446
10	0.2452	0.2045	0.2596	0.2324	0.1520	0.2073
11	0.2490	0.1622	0.2513	0.2274	0.1456	0.2220
12	0.1085	0.0813	0.1143	0.1059	0.0654	0.1370
13	0.1539	0.1448	0.1556	0.1565	0.1347	0.1515

Table 6.3: CCI values for each subject for each time state.

Subject	Baseline1	PLR1	Post1	Baseline2	PLR2	Post2
1	0.1470	0.1416	0.1597	0.5058	0.2079	0.3944
2	0.1716	0.1824	0.1710	0.1171	0.1263	0.1764
3	0.1762	0.1443	0.1403	0.0897	0.1320	0.1590
4	0.0515	0.0395	0.0633	0.0671	0.0422	0.0679
5	0.3292	0.1263	0.1994	0.1635	0.1323	0.2292
6	0.2631	0.1478	0.1558	0.1467	0.1427	0.1610
7	0.1153	0.1273	0.2152	0.1226	0.2187	0.1191
8	0.2770	0.1310	0.3190	0.2312	0.1374	0.3345
9	0.2388	0.1440	0.1850	0.1386	0.0970	0.1294
10	0.3391	0.2635	0.4063	0.4008	0.1762	0.3515
11	0.2488	0.1107	0.2035	0.1797	0.0855	0.1884
12	0.0837	0.0639	0.1440	0.0995	0.0523	0.0961
13	0.1385	0.0947	0.1530	0.1232	0.1236	0.1810

Table 6.4: RCI values for each subject for each time state.

Subject	Baseline1	PLR1	Post1	Baseline2	PLR2	Post2
1	17.90	18.92	20.91	7.549	18.00	7.927
2	19.27	20.68	22.56	22.15	28.30	16.58
3	13.83	14.88	14.84	12.68	14.81	17.17
4	21.11	21.04	20.92	21.07	21.52	20.39
5	9.925	18.20	14.58	11.64	17.23	12.56
6	19.55	20.55	18.85	19.41	20.75	19.00
7	10.44	10.05	11.42	11.58	8.25	10.95
8	14.58	14.26	10.97	12.41	13.10	10.26
9	14.45	18.40	14.28	12.25	13.54	13.41
10	5.642	8.001	4.913	5.669	10.41	5.775
11	10.91	15.79	11.64	12.63	16.96	12.82
12	18.31	20.06	17.87	17.79	21.26	16.64
13	10.66	14.47	10.47	10.81	13.95	9.990

Table 6.5: Mean diameter values for each subject for each time state.

The tables were then used to perform a two-way ANOVA for repeated measures. The aim of the analysis was to evaluate three key aspects:

- The main effect of the first factor, such as the time state: The ANOVA allowed us to evaluate whether the differences observed in the measurements carried out in different time states were statistically significant. This allows us to understand how the results of the measurements vary significantly in the different time states, independently of the subjects.

- The main effect of the second factor, such as the subjects: The ANOVA allowed us to evaluate whether the results of the measurements vary significantly between the subjects, independently of the different time states.

- The interaction between the two effects.

The ANOVA returned p-values associated with each effect. If the p-value for each effect was less than a pre-specified threshold (0.05), it was concluded that there were significant differences.
Table 6.6 shows the results of the two-way ANOVA for repeated measures for the CI measures, in particular it shows the p-values for each factor of analysis. It is noted that the p-values below the chosen threshold are two, related to the factors Intercept and (Intercept)States. A p-value less than the significance threshold for the Intercept factor indicates that the intercept, i.e. the overall average effect, is highly significant. This establishes that there is a significant overall difference in the observed results between the factor levels.. The p-value for the Subject factor is instead higher than the significance threshold, i.e., no significant differences were found between subjects. This result indicates that intra-subject variability does not significantly impact the measures.
The (Intercept)States factor represents the interaction between the intercept and the temporal state, and it is found to be highly significant. This result suggests that there is a highly significant effect of the temporal state factor on the result, that is, there are significant differences in the measurements made in the different temporal states. The last row instead shows the p-value for the interaction between the two factors, subject and states. This value is above the significance threshold, which means that the effect of the time state does not vary significantly between different subjects.
The tables 6.7 and 6.8 show the results of the two-way ANOVA for repeated measures for the CCI and RCI measures. These two parameters, as seen for the CI, are significantly influenced by the effect of the temporal states.

Factors	**pValue**
(Intercept)	0.001
Subject	0.534
(Intercept)States	0.001
Subject:States	0.657

Table 6.6: p-values from the two-way ANOVA for repeated measures for the CI measures.

Factors	pValue
(Intercept)	0.004
Subject	0.205
(Intercept)States	0.006
Subject:States	0.203

Table 6.7: p-values from the two-way ANOVA for repeated measures for the CCI measures.

Factors	pValue
(Intercept)	0.002
Subject	0.876
(Intercept)States	0.002
Subject:States	0.712

Table 6.8: p-values from the two-way ANOVA for repeated measures for the RCI measures.

Table 6.9 instead shows the p-values, obtained from the two-way ANOVA for repeated measures, for the mean diameter measurements. Also for the mean diameter measurements, it can be seen from the table that there is a significant baseline effect, that is, the p-value for the intercept is lower than the significance threshold. The same is true for the interaction between intercept and states, whose p-value indicates that also for these measurements there is a significant difference in the measurements when these are performed in different time states. As for the CI, also for the diameters the table shows that no statistically significant differences were found with regard to the effect due to the subjects and that due to the interaction between subjects and time states.

Factors	pValue
(Intercept)	$9.07e^{-06}$
Subject	0.129
(Intercept)States	$1.36e^{-06}$
Subject:States	0.162

Table 6.9: p-values from the two-way ANOVA for repeated measures for the mean diameter measurements.

The analysis performed using the two-way ANOVA for repeated measures has therefore shown how, both for the pulsatility indices and for the mean diameters, the effect due to the different temporal states in which the measurements are performed significantly influences the parameters, while there is no significant effect due to intra-subject variability. In all cases it is also evident how, since there is no significant interaction between the subjects and the temporal states, the effect of

the temporal states is uniform among all the subjects analyzed.
Although ANOVA allowed us to determine that there is a significant effect on the parameters due to the different temporal states, it is not possible to determine, with this method alone, which temporal states are significantly different from others. In fact, ANOVA detects the presence of general differences between the levels of a factor, without specifying between which of the levels there are significant differences. To investigate this aspect, a second analysis was carried out using the pairwise comparison t-test to identify which temporal states differ significantly. The pairwise comparison t-test calculates the mean difference between the measurements taken in two analyzed temporal states, to then evaluate whether this difference is large enough to be significant. To evaluate this, the test returns a p-value that, if lower than a significance threshold (0.05), determines that there is a significant difference, otherwise, determines that it is not possible to state that there is a significant difference in the measurements taken between the two states.
For this analysis, seven pairs of temporal states were evaluated: baseline1-PLR1, baseline2-PLR2, PLR1-post1, PLR2-post2, PLR1-PLR2, baseline1-baseline2, post1-post2. The tables 6.10, 6.11, 6.12 and 6.13 show the p-values for the parameters measured in all the analyzed time pairs. What can be noted is that for all the parameters significant differences were highlighted between the values measured before each maneuver and those measured during the maneuvers.
Only in the case of the RCI, there is no evidence to state that there are significant differences between the values measured before the second maneuver and the values measured during the second maneuver. Even for the comparisons carried out between the values measured during the maneuvers and those measured immediately after them, the test returned p-values lower than the significance threshold, that is, there is a significant difference between measurements taken during and immediately after the two maneuvers. An exception, in this case, is the measurement of the CCI, for which no significant differences are found between the measurements taken during and immediately after the second PLR maneuver.
What is important to note is that the paired t-tests showed that there is not enough evidence to reject the null hypothesis, that is, to state that there are significant differences, in the comparison between all the parameters measured during the two PLR maneuvers. This proves that the measurements remain similar when performed for repeated maneuvers. This result can be interpreted as an indication of the absence of adaptation of the body in response to repeated maneuvers.

Pairs of temporal states	**pValue**
Baseline1-PLR1	0.002
Baseline2-PLR2	0.036
PLR1-post1	0.002
PLR2-post2	0.016
PLR1-PLR2	0.977
Baseline1-baseline2	0.495
Post1-post2	0.936

Table 6.10: Results (p-values) of pairwise t-tests for comparisons between CI measurements performed in each pair of time states.

Pairs of temporal states	pValue
Baseline1-PLR1	0.016
Baseline2-PLR2	0.021
PLR1-post1	0.021
PLR2-post2	0.252
PLR1-PLR2	0.985
Baseline1-baseline2	0.793
Post1-post2	0.544

Table 6.11: Results (p-values) of pairwise t-tests for comparisons between CCI measurements performed in each pair of time states.

Pairs of temporal states	pValue
Baseline1-PLR1	0.009
Baseline2-PLR2	0.087
PLR1-post1	0.003
PLR2-post2	0.009
PLR1-PLR2	0.808
Baseline1-baseline2	0.838
Post1-post2	0.804

Table 6.12: Results (p-values) of pairwise t-tests for comparisons between RCI measurements performed in each pair of time states.

Pairs of temporal states	pValue
Baseline1-PLR1	0.007
Baseline2-PLR2	0.006
PLR1-post1	0.029
PLR2-post2	0.012
PLR1-PLR2	0.791
Baseline1-baseline2	0.462
Post1-post2	0.170

Table 6.13: Results (p-values) of pairwise t-tests for comparisons between mean diameter measurements performed in each pair of time states.

To further confirm these results, the percentage changes in parameters between baseline conditions and PLR maneuvers were analyzed as a final analysis. The changes were then analyzed using statistical tests to evaluate whether the parameters varied differently between the first baseline condition and the first PLR maneuver and the second baseline condition and the second PLR maneuver.
Two statistical methods were used for this analysis, one parametric and one non-parametric, since the changes in pulsatility indices followed a normal distribution, while the changes in diameters did not. Paired t-test was performed to evaluate whether there were significant differences in the changes in pulsatility indices. In-

stead, a Wilcoxon test for paired data was performed to evaluate whether there were significant differences in the changes in mean diameters.
All these statistical tests highlighted how it is not possible, for any of the parameters, to state that there are significant differences, that is, the parameters vary in the same way for repeated PLR maneuvers. This is confirmed to be consistent with the previous statistical tests performed, further demonstrating how the measurements are stable and consistent when performed during subsequent PLR maneuvers.

Chapter 7

Graphical user interface (GUI)

A graphical user interface (GUI) is a type of digital interface that allows the user to interact with the machine through graphical icons, making it easier and more intuitive to use. The interaction is based on the use of visual elements, such as buttons, windows, and icons, rather than simply typing text commands [30]. Since the nature of the graphical user interface is independent of the application functions, it is possible to customize the appearance of an application software as desired [11]. The advantage of using a GUI is improved usability, as features include familiar icons and can be mastered without the need for computer language knowledge [11].

7.1 Development tools

In this thesis work, as a final part, we focused on the graphic development of a possible GUI for the segmentation software developed by Viper s.r.l.. The analysis of the hemodynamic parameters characteristic of the IVC, carried out in this thesis work, was performed using a software developed on the Matlab programming environment, while the GUI developed in this part of the work involves the use of Python as a programming language. Python is known for its many advantages, including:

- It is an open source library, and has a large community that contributes to its development.
- It has extensive support libraries, for example for numerical calculations and data analysis.
- It is a simple, readable and versatile programming language.
- Python offers intuitive and easy-to-use data structures, making it easy to manipulate data even for non-expert programmers.
- Versatile, easy to read, learn and write: Python is known for its simplicity and readability, making it an excellent choice for both beginners and experienced programmers [28].

In particular, among the wide libraries made available by Python, the PyQt library was used for this work. PyQt is a Python library for building GUIs using the Qt toolkit [26]. PyQt is free software, under the GPL, created by Riverbank Computing. The latest version, PyQt6, which uses Qt 6 and was released in 2021, was used for this work [26]. Among the advantages of using PyQt are:

- It is a very powerful framework that allows you to create professional applications.
- It includes many advanced widgets.
- It is a library that has little dependency on third parties, that is, most things can only be done using PyQt.
- It provides ready-to-use GUIs.
- You can find complete support online on its use.
- It is a cross-platform that runs on Windows, Linux, macOS and mobile devices.
- It can take advantage of Qt Designer, a GUI generator that uses a drag-and-drop graphical editor [27].

The tools used for the interface design were PyQt6 and Qt Designer. The latter allows you to create the graphical interface quickly, by defining the layouts and the main widgets, such as buttons, menus and text boxes, all without having to write all the code manually. Once Qt Designer is opened, the main window is automatically generated into which you can drag the elements you want to include in the GUI. The organization of the elements is hierarchical, that is, it is possible to insert the container elements in such a way that they follow a positioning guided by the choice of a specific layout [29]. A layout is a non-visible graphic element that organizes the containers so that they are arranged horizontally, vertically in a grid or in a module between them. By choosing a specific layout it is possible to manage the geometry of the elements to be inserted in the GUI. Each container element, instead, is a particular type of widget that can contain other widgets or layouts. The ease of use of Qt Designer lies in the ability to select widgets and layouts and drag them directly with the mouse into the main window, defining their spatial positioning. Figure 7.2 shows all the possible layout choices proposed by Qt Designer. Figure 7.3 shows all the container elements available in Qt designer, in particular:

- Group Box: is a widget generally used to group collections of buttons or checkboxes that have similar functionality.
- Scroll area: is a widget used to display the content of a child widget inside a frame.
- ToolBox: are widgets that provide a series of compartments in a toolbox.
- Tab Widgets: allow you to split the content of a widget into two distinct and labeled sections, only one visible at a time.

- Stacked Widgets: are collections of widgets in which only the top level is visible. Usually there is an additional widget that manages control over the visible level.
- Frame: are widgets used as visual containers, capable of containing other widgets. They are used to be able to visually separate elements from others in the interface.
- MDI area: works as an MDI window manager.
- Dock Widgets: These are floating panels that attach to the edges of the main window in "dock areas", or float as independent tool windows [41].

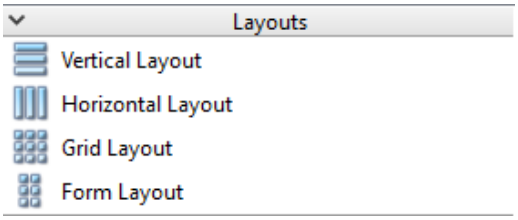

Figure 7.1: Layouts Panel in Qt Designer.

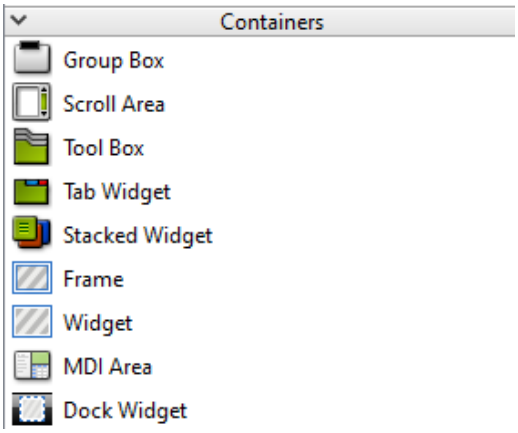

Figure 7.2: Widget containers in Qt Designer.

7.2 GUI concept

The aim was to propose an interface that would allow for simpler and more intuitive use and that would include all the functions necessary to perform the correct segmentation of the inferior vena cava (IVC).
The figure 7.1 shows a diagram that indicates the main elements that are considered essential for the purposes of the analysis. From the diagram, it is clear that the GUI designed includes a menu bar through which it is possible to select multiple analysis

modes, depending on whether the ultrasound video to be analyzed is a transverse or longitudinal view of the IVC. In addition, for each viewing mode, the possibility of segmenting a previously acquired video (post processing) or acquiring and segmenting a video in real time (new video) is included. The menu bar also includes a function that allows you to save the segmented video and one that allows you to select the language in which you want to use the software.
It is also necessary that there is a panel of the parameters that you want in output from the segmentation. The purpose of the IVC segmentation is to follow the upper and lower edges of the IVC and then calculate the maximum, minimum and average diameter for each frame of the ultrasound, and then proceed to calculate the pulsatility indices. Through this panel it is possible to select the parameters that you want to obtain, divided into default parameters, that is, the parameters that are always defined in output, and optional parameters, such as CCI and RCI, which can be selected manually for more in-depth analysis.
Finally, the GUI must necessarily contain two other main sections, one that gives the possibility of viewing the ultrasound video in order to allow the user to manually carry out all the steps necessary for segmentation (Video Section), and one that allows viewing the trend of the output parameters (Graphic Section).

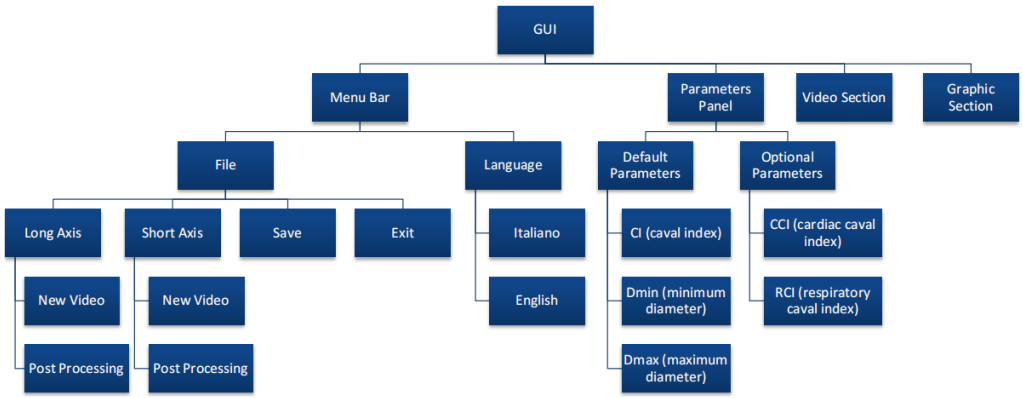

Figure 7.3: Block chart showing the elements included in the GUI.

Before proceeding to create the GUI on Python, a prototype was made by hand to define a first idea of graphics and organize in space all the tools needed to ensure a good functioning of the interface. The model is shown in the figures 7.4 and 7.5 and contains most of the tools that were then inserted into the final GUI. Some additional tools, not present in the initial model, were then added in the actual development phase.

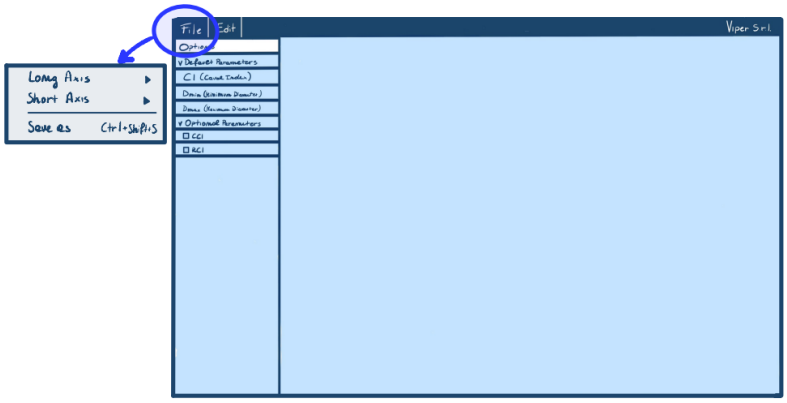

(a)

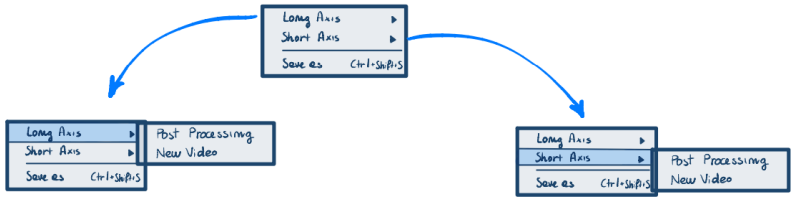

(b)

Figure 7.4: Model.

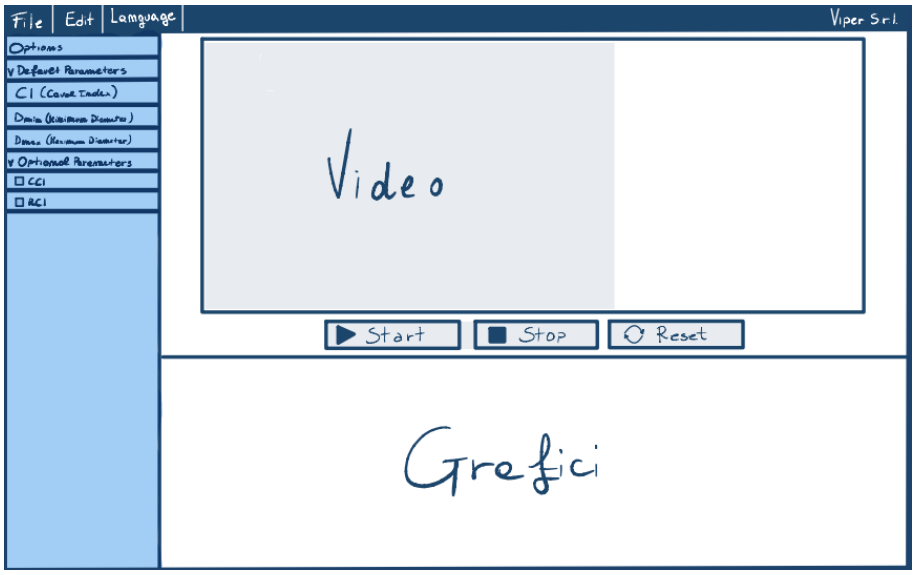

Figure 7.5: Final Model.

Using the template as a guide, we proceeded to create the GUI on Python, using PyQt6 and Qt Designer, section by section.
The toolbar was created using the *Qmenubar* widget, a container that can contain

different objects, called *Qmenu*, within which different actions have been inserted, that is, menu items linked to specific actions. The objects inserted in the toolbar are: File and Language. By selecting the File item, it is possible to display the ultrasound video display options, short axis and long axis, together with the option to save the segmented video (figure 7.4). By selecting the Language item, it is possible to choose between two languages: English or Italian.

Figure 7.6: "File" item in the menu bar.

For both viewing modes, you can then select a previously acquired video using the "post processing" action or acquire a new video in real time using the "new video" action (figure 7.4).

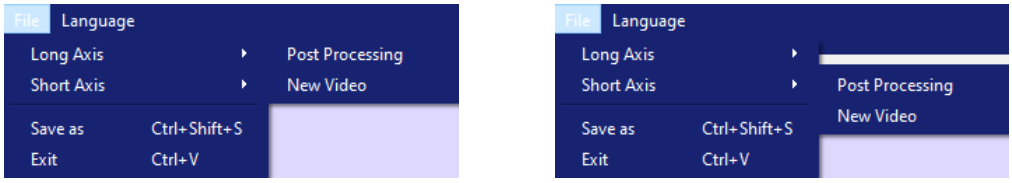

(a) (b)

Figure 7.7: Ultrasound video selection menu.

Another feature of the GUI is the parameters panel, created with an element widget, called *TreeView*, which allows you to create a simple tree-like structure of the model. This widget stores data internally to the model using *Treeitem* objects, linked together via a pointer-based tree structure. Each *Treeitem* has a parent element and a number of child elements. In this project, there are two parent *Treeitems*, default parameters and optional parameters, each with its own child elements [37].
In figure 6.7 (b) you can see how a checkbox has been added to the optional parameters, using the *setCheackable*(*true*) method, which makes them selectable. This allows the user to manually decide whether or not to include these parameters in the analysis.

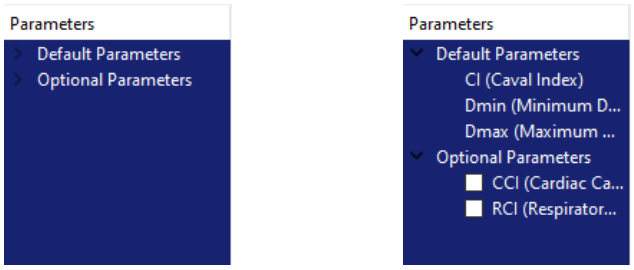

(a) (b)

Figure 7.8: Parameters panel.

The last two elements are those that include the possibility of viewing the ultrasound video of the IVC to be segmented and the possibility of viewing the trend of the average diameters during the duration of the video clip.
For the viewing of the ultrasound video, a $Qframe$ class object was first inserted that allows the creation of an element visible in the main window. An image viewing widget, *Qlabel*, was then inserted inside the $Qframe$, within which the video clip can then be played (figure 7.7). In the figure, some widgets are also visible, *Qpushbutton*, which allow the generation of clickable buttons, specifically, capable of starting the analysis (start), ending the analysis (stop) and resetting the analysis from the beginning (reset).

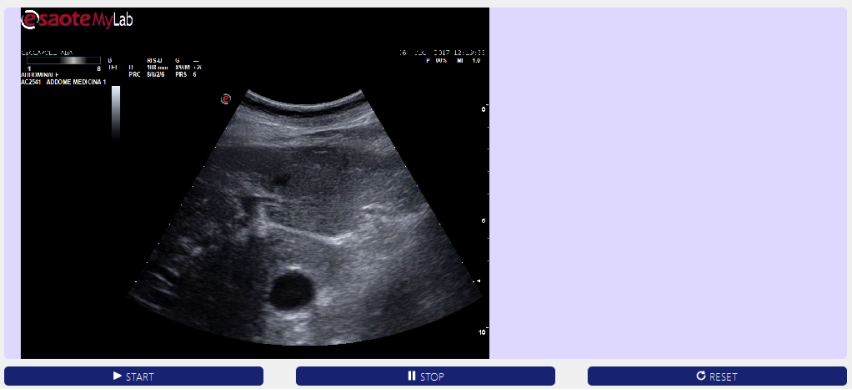

Figure 7.9: Element for viewing the ultrasound video and buttons for controlling the analysis.

Figure 7.8, instead, shows the graph containing the values of the average diameters calculated for each frame, generated using *pyqtgraph*, a Python library based on PyQt and *QtGraph*. The graph is contained within a $Qframe$ specifically created to contain it.

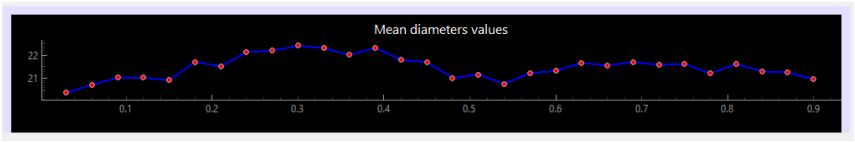

Figure 7.10: Element for viewing the graph containing the values of the average diameters calculated for each frame.

Figure 7.9 shows the final GUI, containing all the elements described above.

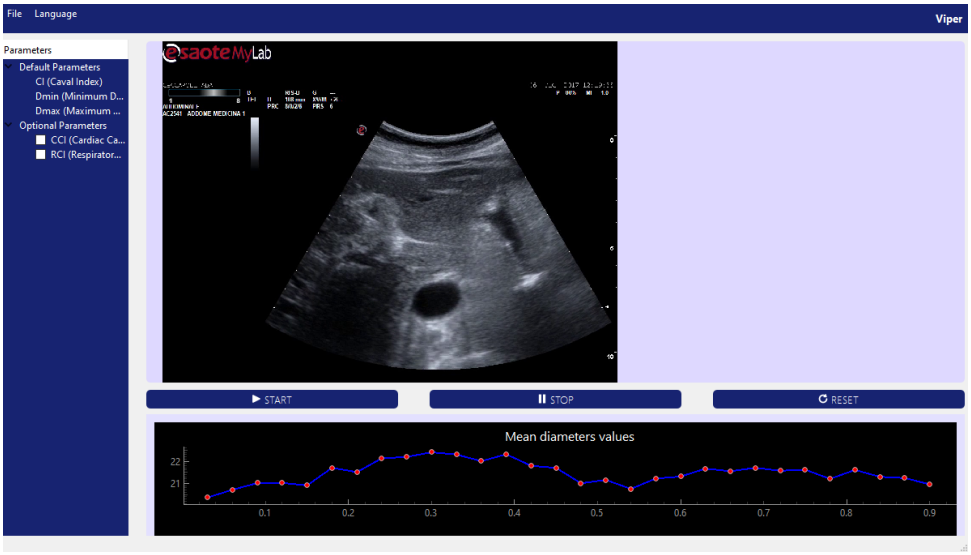

Figure 7.11: Final graphical user interface (GUI).

Chapter 8

Conclusions

The aim of this study was to evaluate the effect of repeated PLR maneuvers on hemodynamic parameters, such as pulsatility indices and mean diameters of the inferior vena cava, starting from a dataset of thirteen subjects. In particular, considering each maneuver composed of three time intervals, before, during and after, it was evaluated whether there were significant differences between the parameters measured in the different temporal states.
Different statistical analyses allowed to determine whether a physiological adaptation to repeated maneuvers occurred, or if, instead, the measures were stable over time. The two-way ANOVA for repeated measures highlighted how there was a significant difference between the parameters when these were measured in different temporal states, therefore how the effect of time influenced the hemodynamic measures. However, no significant differences in the measures were found between the different subjects.
Since ANOVA could not be used to investigate more precisely which temporal states most significantly affected the measurements, paired t-tests were performed to investigate differences in measurements made between specific pairs of temporal states.
This analysis showed that parameters differ significantly when measured before and during the PLR maneuvers, as well as during and after them. However, no significant differences were found between parameters when the two maneuvers were directly compared. This led to the conclusion that there is a lack of adaptation of parameters in response to repeated maneuvers.
Further statistical tests confirmed these results, determining how parameters varied very similarly between the baseline condition and the PLR for both maneuvers.
It can therefore be concluded that the measurements made during the two PLR maneuvers are stable and consistent between the two analysis sessions.
The results are relevant as they suggest that it is possible to perform repeated maneuvers without compromising the significance or reliability of the data obtained. It can therefore be assumed that the response observed through the analyzed hemodynamic parameters is constant and reproducible. This provides a solid basis for the use of the maneuver in subsequent studies or in clinical settings that require the repeatability of the procedure.

Appendix A

Additional Images

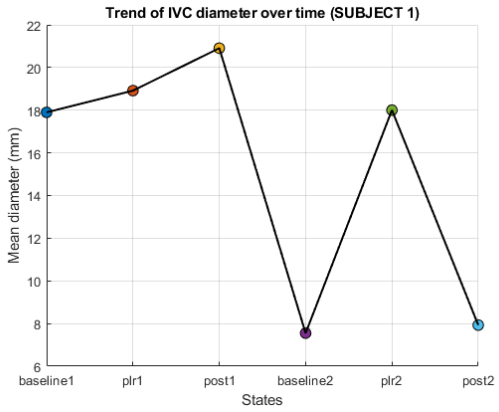

(a) Trend of mean diameter values of subject 1 during baseline, PLR and post-maneuvers for both PLR maneuvers.

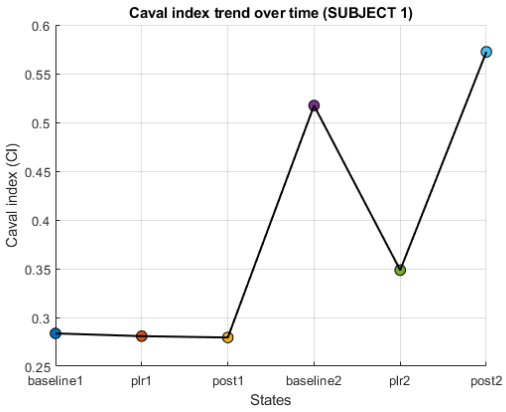

(b) Trend of CI values of subject 1 during baseline, PLR and post-maneuvers for both PLR maneuvers.

Figure A.1: Trend of the mean IVC diameter and pulsatility index (CI) over the time of the subject 1.

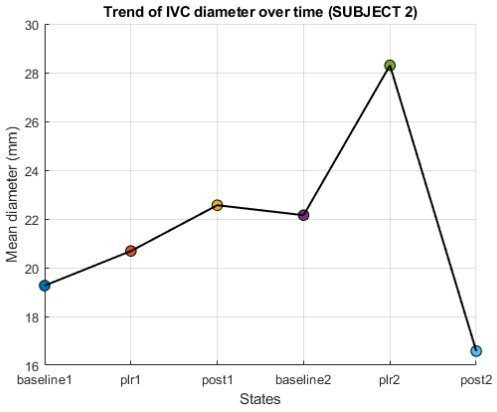

(a) Trend of mean diameter values of subject 2 during baseline, PLR and post-maneuvers for both PLR maneuvers.

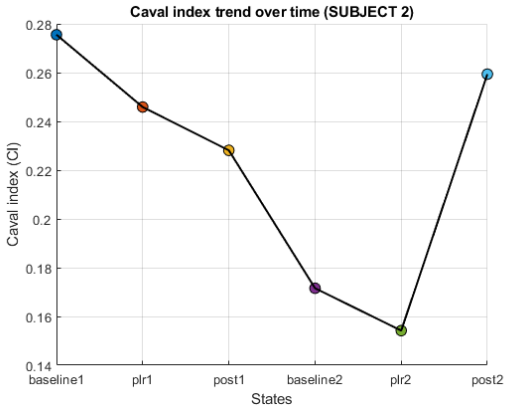

(b) Trend of CI values of subject 2 during baseline, PLR and post-maneuvers for both PLR maneuvers.

Figure A.2: Trend of the mean IVC diameter and pulsatility index (CI) over the time of the subject 2.

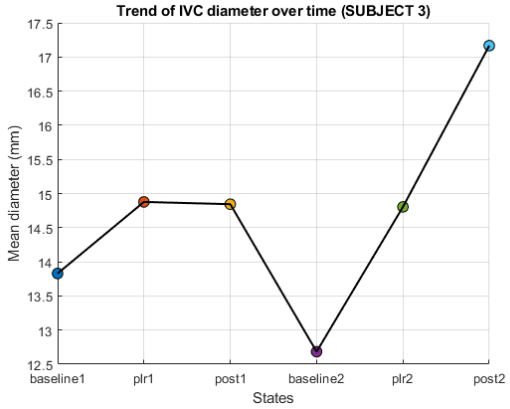

(a) Trend of mean diameter values of subject 3 during baseline, PLR and post-maneuvers for both PLR maneuvers.

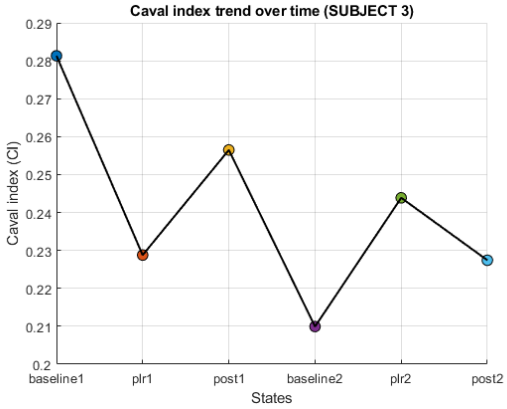

(b) Trend of CI values of subject 3 during baseline, PLR and post-maneuvers for both PLR maneuvers.

Figure A.3: Trend of the mean IVC diameter and pulsatility index (CI) over the time of the subject 3.

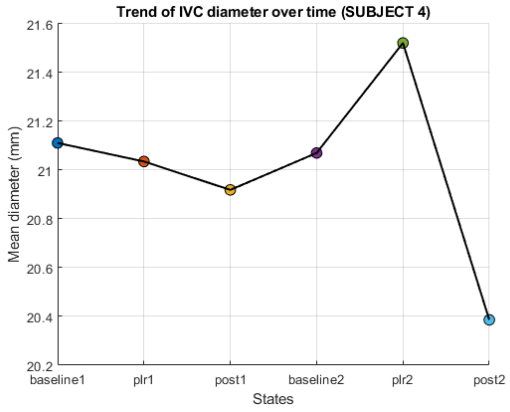

(a) Trend of mean diameter values of subject 4 during baseline, PLR and post-maneuvers for both PLR maneuvers.

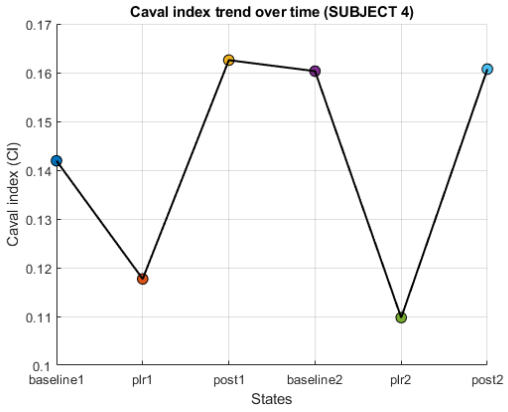

(b) Trend of CI values of subject 4 during baseline, PLR and post-maneuvers for both PLR maneuvers.

Figure A.4: Trend of the mean IVC diameter and pulsatility index (CI) over the time of the subject 4.

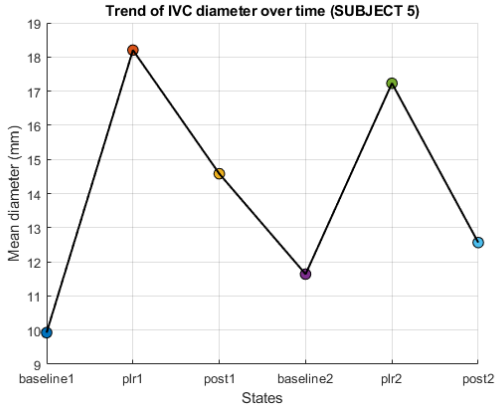

(a) Trend of mean diameter values of subject 5 during baseline, PLR and post-maneuvers for both PLR maneuvers.

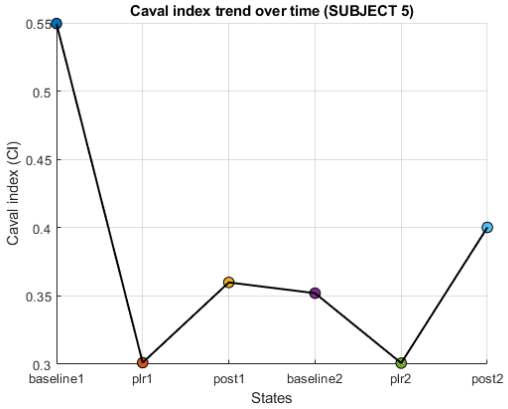

(b) Trend of CI values of subject 5 during baseline, PLR and post-maneuvers for both PLR maneuvers.

Figure A.5: Trend of the mean IVC diameter and pulsatility index (CI) over the time of the subject 5.

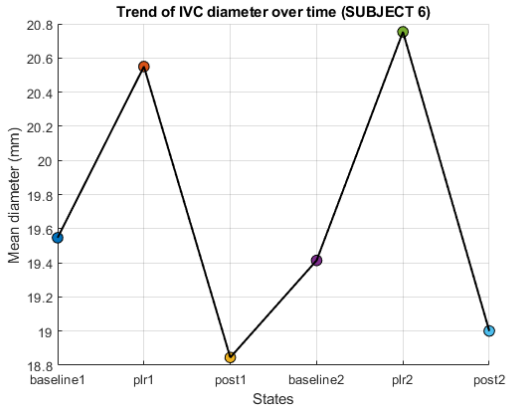

(a) Trend of mean diameter values of subject 6 during baseline, PLR and post-maneuvers for both PLR maneuvers.

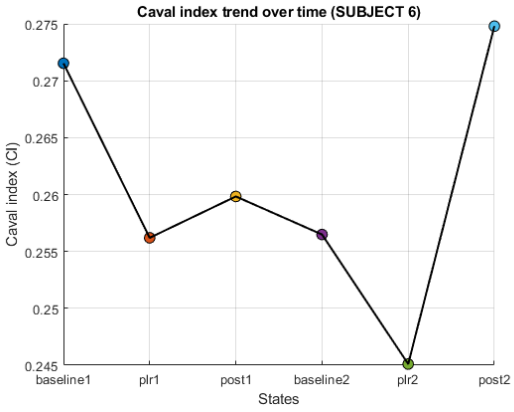

(b) Trend of CI values of subject 6 during baseline, PLR and post-maneuvers for both PLR maneuvers.

Figure A.6: Trend of the mean IVC diameter and pulsatility index (CI) over the time of the subject 6.

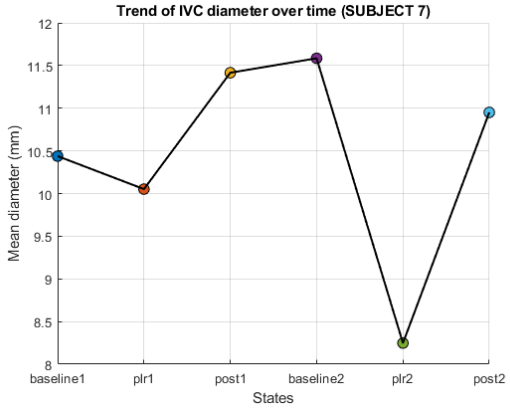

(a) Trend of mean diameter values of subject 7 during baseline, PLR and post-maneuvers for both PLR maneuvers.

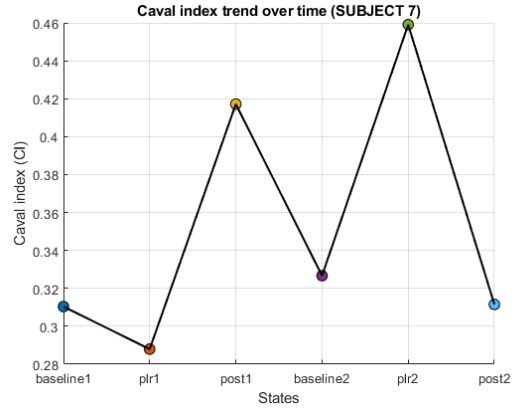

(b) Trend of CI values of subject 7 during baseline, PLR and post-maneuvers for both PLR maneuvers.

Figure A.7: Trend of the mean IVC diameter and pulsatility index (CI) over the time of the subject 7.

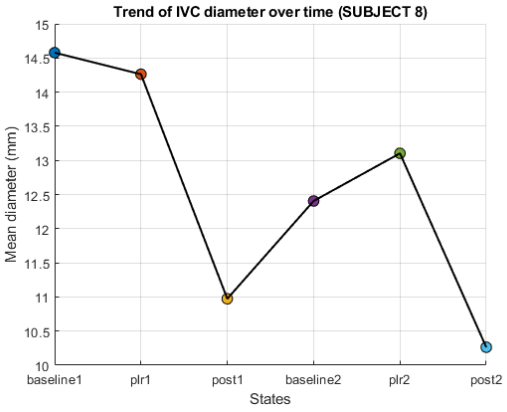

(a) Trend of mean diameter values of subject 8 during baseline, PLR and post-maneuvers for both PLR maneuvers.

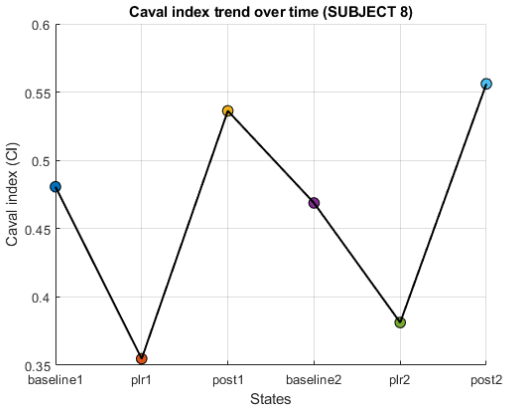

(b) Trend of CI values of subject 8 during baseline, PLR and post-maneuvers for both PLR maneuvers.

Figure A.8: Trend of the mean IVC diameter and pulsatility index (CI) over the time of the subject 8.

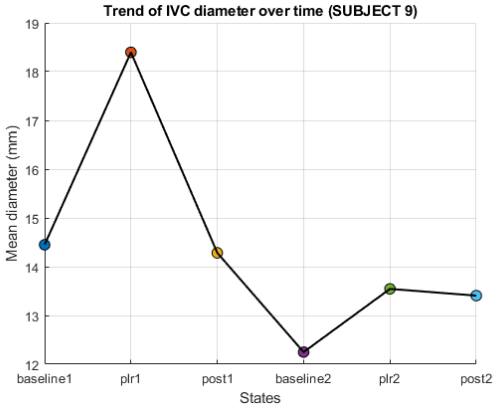

(a) Trend of mean diameter values of subject 9 during baseline, PLR and post-maneuvers for both PLR maneuvers.

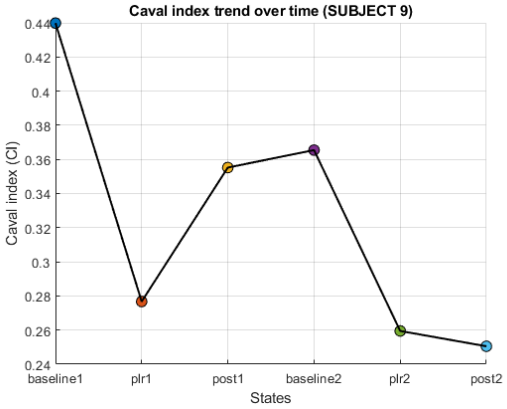

(b) Trend of CI values of subject 9 during baseline, PLR and post-maneuvers for both PLR maneuvers.

Figure A.9: Trend of the mean IVC diameter and pulsatility index (CI) over the time of the subject 9.

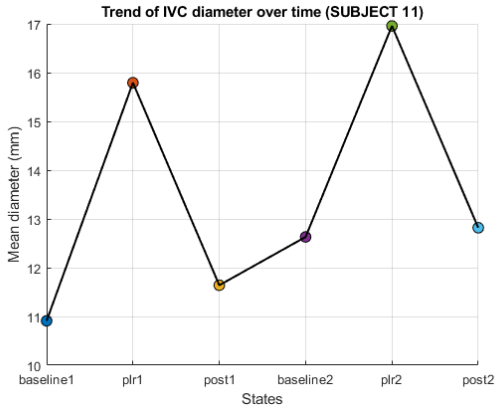

(a) Trend of mean diameter values of subject 11 during baseline, PLR and post-maneuvers for both PLR maneuvers.

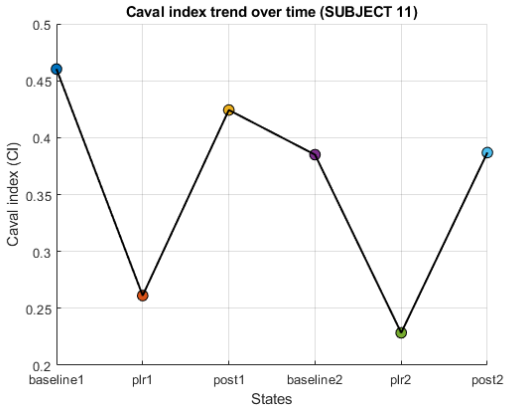

(b) Trend of CI values of subject 11 during baseline, PLR and post-maneuvers for both PLR maneuvers.

Figure A.10: Trend of the mean IVC diameter and pulsatility index (CI) over the time of the subject 11.

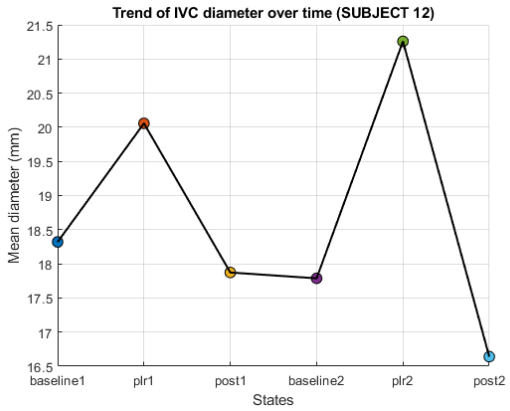

(a) Trend of mean diameter values of subject 12 during baseline, PLR and post-maneuvers for both PLR maneuvers.

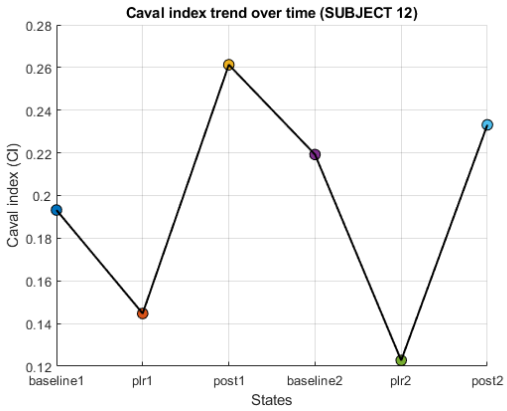

(b) Trend of CI values of subject 12 during baseline, PLR and post-maneuvers for both PLR maneuvers.

Figure A.11: Trend of the mean IVC diameter and pulsatility index (CI) over the time of the subject 12.

Bibliography

[1] *The Process of Breathing*. Anatomy Physiology.

[2] *Respiratory Function: Pressure and Mechanisms of Breathing*. Introductory Animal Physiology 2nd Edition.

[3] How the lungs work. the respiratory system. *National Heart, Lung, and Blood Institute*, 2022.

[4] The a, b, ms – ultrasound modes explained. *imv imaging*, 2023.

[5] `https://it.mathworks.com/help/stats/boxplot.html`.

[6] Amy Brown. The superior vena cava. *teachmeanatomy*, 2020.

[7] `https://simplemed.co.uk/subjects/cardiovascular/anatomy-of-the-cardiovascular-system`.

[8] *Structure and Function of Blood Vessels*, Anatomy and Physiology II.

[9] Keith Corl, Anthony M Napoli, and Fenwick Gardiner. Bedside sonographic measurement of the inferior vena cava caval index is a poor predictor of fluid responsiveness in emergency department patients. *Emergency Medicine Australasia*, 2012.

[10] Leonardo Ermini, Stefano Seddone, Piero Policastro, Luca Mesin, Paolo Pasquero, and Silvestro Roatta. The cardiac caval index: Improving noninvasive assessment of cardiac preload. *Journal of Ultrasound in Medicine*, 2021.

[11] `https://www.heavy.ai/technical-glossary/graphical-user-interface`.

[12] Tim Harris, Timothy J Coats, and Mohammed H Elwan. Fluid therapy in the emergency department: an expert practice review. *Emergency Medicine Journal*, 2018.

[13] Adam Hayes. Two-way analysis of variance (anova): What it is, what it tells you, vs. one-way. *investopedia*, 2024.

[14] Humanitas research Hospital. Vena cava inferiore.

[15] Elaine M Kaptein and Matthew J Kaptein. Inferior vena cava ultrasound and other techniques for assessment of intravascular and extravascular volume: an update. *Clinical Kidney Journal*, 2023.

[16] Thierry Lefevre, Benoit Mory, and Roberto Ardon; Javier Sanchez-Castro; Anthony Yezzi. Automatic inferior vena cava segmentation in contrast-enhanced ct volumes. *2010 IEEE International Symposium on Biomedical Imaging: From Nano to Macro*, 2010.

[17] Manu L. N. G. Malbrain, Thomas Langer, Djillali Annane, Luciano Gattinoni, Paul Elbers, Inneke De laet Robert G. Hahn, Andrea Minini, Can Ince Adrian Wong, David Muckart, Monty Mythen, and Pietro Caironi Niels Van Regenmortel. Intravenous fluid therapy in the perioperative and critical care setting: Executive summary of the international fluid academy (ifa). *Ann. Intensive Care*, 2020.

[18] Paul E Marik, Michael Baram, and Bobbak Vahid. Does the central venous pressure predict fluid responsiveness? an updated meta-analysis and a plea for the abandonment of this practice. *National library of medicine*, 2008.

[19] RONALD B. HIMELMAN MD, BARBARA KIRCHER MD, DON C. ROCKEY MD, and NELSON B. SCHILLER MD FACC. Inferior vena cava plethora with blunted respiratory response: A sensitive echocardiographic sign of cardiac tamponade. *Journal of the American College of Cardiology*, 1988.

[20] Xaime García MD, Peter Simon MD, Francis X. Guyette MD, Ravi Ramani MD, Rene Alvarez MD, Jorge Quintero MD, and Michael R. Pinsky MD FCCP. Noninvasive assessment of acute dyspnea in the ed. *CHEST*, 2013.

[21] Anthony A. Mercadante and Avais Raja. Anatomy, arteries. *National library of medicine*, 2023.

[22] Andrea Minini, Paul Abraham, and Manu L. N. G. Malbrain. Predicting fluid responsiveness with the passive leg raising test: don't be fooled by intra-abdominal hypertension! *Annals of translational medicine*, 2020.

[23] Xavier Monnet and Jean-Louis Teboul. Passive leg raising: five rules, not a drop of fluid! *BCM*, 2015.

[24] Xavier Monnet and Rui Shi Jean-Louis Teboul. Prediction of fluid responsiveness. what's new? *Annals of Intensive Care*, 2022.

[25] Chris Nickson. Passive leg raise. *Life in the fastlane*, 2020.

[26] `https://www.pythonguis.com/pyqt6-tutorial/`.

[27] `https://www.pythonguis.com/faq/pyqt-vs-tkinter/#the-pyqt-gui-framework`.

[28] `https://www.geeksforgeeks.org/python-language-advantages-applications/`.

[29] *Disegnare interfacce con Qt Designer*, 2018.

[30] Linda Rosencrance. Graphical user interface (gui). *Techopedia*, 2024.

[31] Parth Shah and Martine A. Louis. Physiology, central venous pressure. *National library of medicine*, 2023.

[32] Laerd statistics. Wilcoxon Signed-Rank Test using SPSS Statistics.

[33] Michael B. Stone and Jennifer V. Huang. Inferior vena cava assessment: Correlation with cvp and plethora in tamponade. *ScienceDirect*, 2013.

[34] Xavier Monnet Jean-Louis Teboul. Passive leg raising. *Applied Physiology in Intensive Care Medicine 2. Springer*, 2012.

[35] Kent State University. Paired Samples t Test.

[36] Statistics Knowledge Portal. The t-Test.

[37] `https://doc.qt.io/qt-6/qtwidgets-itemviews-simpletreemodel-example.html`.

[38] William D. Tucker, Yingyot Arora, and Kunal Mahajan. Anatomy, blood vessels. *National library of medicine*, 2023.

[39] Carmit Shiran MD PoC Ultrasound, GE Healthcare In collaboration with Lior Fuchs, MD Medical Intensive Care Unit, Soroka University Medical Center, and IL Beersheva. Auto tool for measuring ivc collapsibility index. *GE healthCare*, 2022.

[40] `https://www.viper.srl/`.

[41] *Using Containers in Qt Widgets Designer*.